Crystal Structures of Substrate and Substrate Analog Complexes of Protocatechuate 3,4-Dioxygenase: Endogenous Fe^{3+} Ligand Displacement in Response to Substrate Binding[†,‡]

Allen M. Orville,[§] John D. Lipscomb,* and Douglas H. Ohlendorf*

Department of Biochemistry, Medical School, and Center for Metals in Biocatalysis, University of Minnesota, Minneapolis, Minnesota 55455-0347

Received March 3, 1997; Revised Manuscript Received June 16, 1997[⊗]

ABSTRACT: Protocatechuate 3,4-dioxygenase (3,4-PCD) utilizes a ferric ion to catalyze the aromatic ring cleavage of 3,4-dihydroxybenzoate (PCA) by incorporation of both atoms of dioxygen to yield β-carboxy-*cis,cis*-muconate. The crystal structures of the anaerobic 3,4-PCD·PCA complex, aerobic complexes with two heterocyclic PCA analogs, 2-hydroxyisonicotinic acid *N*-oxide (INO) and 6-hydroxynicotinic acid *N*-oxide (NNO), and ternary complexes of 3,4-PCD·INO·CN and 3,4-PCD·NNO·CN have been determined at 2.1−2.2 Å resolution and refined to *R*-factors between 0.165 and 0.184. PCA, INO, and NNO form very similar, asymmetrically chelated complexes with the active site Fe^{3+} that result in dissociation of the endogenous axial tyrosinate Fe^{3+} ligand, Tyr447 (147β). After its release from the iron, Tyr447 is stabilized by hydrogen bonding to Tyr16 (16α) and Asp413 (113β) and forms the top of a small cavity adjacent to the C3−C4 bond of PCA. The equatorial Fe^{3+} coordination site within this cavity is unoccupied in the anaerobic 3,4-PCD·PCA complex but coordinates a solvent molecule in the 3,4-PCD·INO and 3,4-PCD·NNO complexes and CN^- in the 3,4-PCD·INO·CN and 3,4-PCD·NNO·CN complexes. This shows that an O_2 analog can occupy the cavity and suggests that electrophilic O_2 attack on PCA is initiated from this site. Both the dissociation of the endogenous Tyr447 and the expansion of the iron coordination sphere are novel features of the 3,4-PCD·substrate complex which appear to play essential roles in the activation of substrate for O_2 attack. Together, the structures presented here and in the preceding paper [Orville, A. M., Elango, N., Lipscomb, J. D., & Ohlendorf, D. H. (1997) *Biochemistry 36*, 10039−10051] provide atomic models for several steps in the reaction cycle of 3,4-PCD and related Fe^{3+}-containing dioxygenases.

Many divergent soil bacteria express dioxygenases that catalyze the oxidative aromatic ring cleavage of catechol and its derivatives such as PCA[1] [for reviews, see Lipscomb and Orville (1992) and Que and Ho (1996)]. These are the key enzymes in the aerobic biodegradative pathways that allow the organisms to derive all their carbon and energy from aromatic hydrocarbons (Dagley, 1977, 1978; Harayama et al., 1992). Catecholic dioxygenases are subdivided into two classes on the basis of the site of aromatic ring cleavage and the oxidation state of the catalytically essential metal ion. Extradiol dioxygenases utilize a mononuclear Fe^{2+} or Mn^{2+} to catalyze cleavage of the ring adjacent to the vicinal hydroxyl groups, while intradiol dioxygenases employ Fe^{3+} to catalyze ring opening between the hydroxyl groups. The extradiol dioxygenases apparently activate molecular oxygen by allowing it to bind directly to the Fe^{2+} (Arciero & Lipscomb, 1986; Mabrouk et al., 1991; Shu et al., 1996). In contrast, spectroscopic data obtained from the intradiol dioxygenases in semistable states trapped during turnover, or from ligand complexes thought to mimic intermediate steps during catalysis, indicate that the iron remains high-spin ferric throughout the reaction cycle and thus cannot bind and activate O_2 directly (Fujisawa et al., 1971, 1972; Que et al., 1976; Bull et al., 1981; May et al., 1982; Whittaker et al., 1984; Whittaker & Lipscomb, 1984b). As an alternative mechanism, we have proposed that the intradiol-cleaving dioxygenases activate the catecholic substrates by chelating them as dianions to the Fe^{3+} which promotes direct electrophilic attack by oxygen (Scheme 1) (Lipscomb & Orville, 1992).

[†] This work was supported by grants from the National Institutes of Health to D.H.O. (GM-46436) and to J.D.L. (GM-24689). A.M.O. acknowledges a NIH predoctoral training grant (GM-07323) and a Doctoral Dissertation Fellowship from the Graduate School of the University of Minnesota.

[‡] The coordinates for the 3,4-PCD complexes have been deposited in the Brookhaven Protein Data Bank (Bernstein et al., 1977) with the following identifiers: 3,4-PCD·PCA, 3PCA; 3,4-PCD·INO, 3PCJ; 3,4-PCD·NNO, 3PCK; 3,4-PCD·INO·CN, 3PCL; and 3,4-PCD·NNO·CN, 3PCM.

* Corresponding authors. Douglas H. Ohlendorf, Department of Biochemistry, 4-225 Millard Hall, University of Minnesota, Minneapolis, MN 55455-0347. Telephone: (612) 624-8436. Fax: (612) 625-2163. E-mail: ohlen@dccc.med.umn.edu. John D. Lipscomb, Department of Biochemistry, 4-225 Millard Hall, University of Minnesota, Minneapolis, MN 55455-0347. Telephone: (612) 625-6454. Fax: (612) 625-2163. E-mail: lipsc001@maroon.tc.umn.edu.

[§] Current address: Institute of Molecular Biology, University of Oregon, Eugene, OR 97403.

[⊗] Abstract published in *Advance ACS Abstracts,* August 1, 1997.

[1] Abbreviations: 3,4-PCD, protocatechuate 3,4-dioxygenase; 1,2-CTD, catechol 1,2-dioxygenase; Cl-CTD, chlorocatechol 1,2-dioxygenase; PCA, protocatechuate or 3,4-dihydroxybenzoate; HPCA, homoprotocatechuate or 3,4-dihydroxyphenylacetate; FHB, 3-fluoro-4-hydroxybenzoate; IHB, 3-iodo-4-hydroxybenzoate; INO, 2-hydroxyisonicotinic acid *N*-oxide; NNO, 6-hydroxynicotinic acid *N*-oxide; TPA, tris(2-pyridylmethyl)amine; DHB, 3,5-di-*tert*-butylcatecholate dianion; EPR, electron paramagnetic resonance; XANES, x-ray absorption near edge structure; EXAFS, extended X-ray absorption fine structure; LMCT, ligand to metal charge transfer; rms, root mean squared; F_P, $F_{P\cdot PCA}$, $F_{P\cdot INO}$, $F_{P\cdot NNO}$, $F_{P\cdot INO\cdot CN}$, and $F_{P\cdot NNO\cdot CN}$, observed structure factors for the uncomplexed or complexed 3,4-PCD.

S0006-2960(97)00469-8 CCC: $14.00

Scheme 1: Proposed Reaction Mechanism of 3,4-PCD Highlighting a PCA Tautomer Activated for Electrophilic Attack by O_2 (Lipscomb & Orville, 1992)[a]

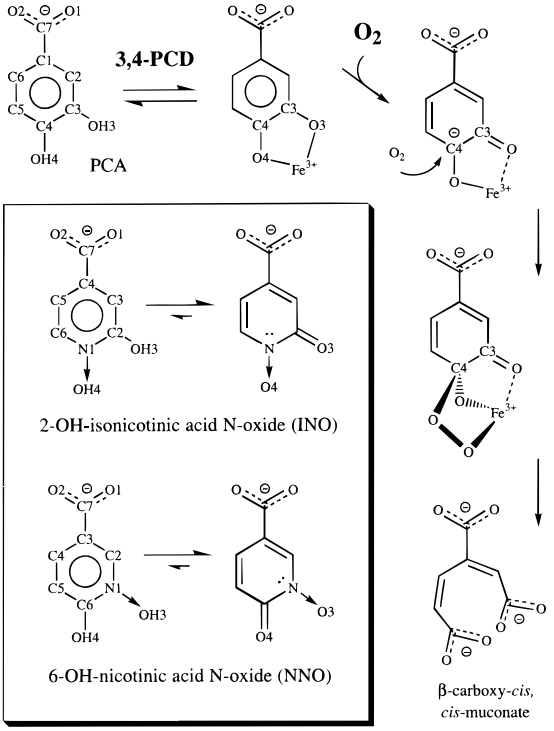

[a] (Inset) INO and NNO are analogs of the ketonized substrate (Whittaker & Lipscomb, 1984b).

Crystallographic and spectroscopic studies show that the active site Fe^{3+} of protocatechuate 3,4-dioxygenase (3,4-PCD), an archetypal intradiol dioxygenase, is coordinated in a distorted trigonal bipyramid ligand geometry in which Tyr447$^{O\eta}$ and His462$^{N\epsilon 2}$ provide the axial ligands[2] while Tyr408$^{O\eta}$, His460$^{N\epsilon 2}$, and a solvent hydroxide ion (Wat827) form the equatorial ligands (Ohlendorf et al., 1988, 1994; Lipscomb & Orville, 1992; Felton et al., 1984; True et al., 1990). The two tyrosinate ligands are thought to stabilize the ferric ion and give 3,4-PCD its characteristic burgundy-red color via ligand to metal charge transfer (LMCT) electronic transitions (Que, 1989). The preceding paper presented crystal structures of seven competitive inhibitor complexes of 3,4-PCD (Orville et al., 1997). The structures of the monohydroxybenzoate and 3-halo-4-hydroxybenzoate complexes (Orville et al., 1997) showed that these inhibitors form monodentate Fe^{3+} complexes through the C4-phenolate group in accord with previous spectroscopic results (Orville & Lipscomb, 1989). Although Wat827 was either shifted or displaced in each of these complexes, the four endogenous iron ligands remained essentially unchanged by complex formation. Since the competitive inhibitors utilized in the previous study have only one phenolate group, they could not mimic the proposed chelated substrate complex that we believe to be essential for catalysis. However, they do suggest a logical set of orientations that the substrate might assume during the binding process beginning with the resting state of the enzyme.

The evidence for a chelated PCA·Fe^{3+} complex has been derived largely from spectroscopic studies. EPR and Mössbauer spectra of substrate complexes are very complex, indicating that several binding orientations are possible in solution. However, the EPR spectrum of the dominant form (>90% for the complex with 3,4-dihydroxyphenylacetate, an alternative substrate) is broadened by superhyperfine interactions when ^{17}O is incorporated into either of the catecholic oxygen atoms, implying that both are bound to the iron (Orville & Lipscomb, 1989). Similar studies using ^{17}O-enriched water showed that the solvent is bound to the iron in the absence of substrates but is apparently displaced when substrates are added (Whittaker & Lipscomb, 1984a; Orville & Lipscomb, 1989). Interestingly, XANES and EXAFS studies indicate that the Fe^{3+} remains five-coordinate in the substrate·chelate complex, indicating that one of the endogenous iron ligands is displaced in addition to the solvent ligand (True et al., 1990). Therefore, the spectroscopic data suggested that substrate chelation engenders a change in the endogenous iron coordination sphere.

The process of substrate binding and its conformation during catalysis have been studied by transient kinetic studies of PCA turnover (Fujisawa et al., 1971, 1972; Bull et al., 1981) and by the binding of two heterocyclic substrate analogs, INO and NNO. The latter *N*-oxide inhibitors were developed to mimic the ketonized tautomers of PCA (Scheme 1) which is believed to form just prior to, or coincident with, attack of oxygen on the ionized substrate (Lipscomb et al., 1982; May et al., 1982; Whittaker & Lipscomb, 1984b). Significantly, the transient kinetic studies showed that these analogs passed through at least three enzyme-associated states before finally forming the complex involving the ketonized tautomer. This final state was characterized by a loss of the burgundy color of the enzyme and strongly resembled an intermediate observed in the natural catalytic cycle immediately after addition of O_2 to the anaerobic 3,4-PCD·-PCA complex (Bull et al., 1981). EPR-detected superhyperfine broadening from the ^{17}O-labeled solvent indicated that the solvent is displaced from the iron in the early INO and NNO intermediates but rebinds in the final bleached complex (Whittaker & Lipscomb, 1984a). Together, these experiments provided the first evidence that the ligand sphere of the active site Fe^{3+} changes dynamically during turnover.

Cyanide is another inhibitor of 3,4-PCD and has also been used to probe the active site Fe^{3+} ligation and the effects of substrate or inhibitor binding. In the absence of substrate-like molecules, cyanide binds to 3,4-PCD·Fe^{3+} in a complex process involving at least two cyanide molecules (Orville & Lipscomb, 1989). In the presence of PCA, spectroscopic and kinetic evidence suggested that CN^- binding is complex and alters the electronic properties of the substrate·Fe^{3+} complex to yield homogeneous EPR and Mössbauer spectra (Whittaker & Lipscomb, 1984a; Orville & Lipscomb, 1989). X-ray crystallographic studies of the 3,4-PCD·PCA·CN complex would be valuable as a potential model for O_2 binding in the active site. However, the 3,4-PCD·PCA·CN complex is a transient species that decays to the same dead end species as was observed for CN^- binding in the absence of substrate. Fortunately, CN^- was observed to bind similarly to the 3,4-PCD·INO and 3,4-PCD·NNO complexes (Whittaker & Lipscomb, 1984a) to yield more stable ternary

[2] With the exception of Figure 9, the amino acid residue numbering scheme is that utilized in the refinement of the 3,4-PCD as isolated from *Pseudomonas putida* (Ohlendorf et al., 1994): α-Subunits (residues 1−200), *β*-subunits (residues 301−538). A substrate or substrate analog within the active site and a 3-fold site are numbered 550 and 551, respectively. CN^- is residue 575; iron is residue 600, and solvent numbering starts at 601.

Table 1: Summary of Data Collection and Atomic Model Refinement Statistics

data collection					
ligand (concentration)	PCA (70 mM)[a]	INO (2 mM)	NNO (40 mM)	INO (20 mM) + NaCN (200 mM)	NNO (20 mM) + NaCN (200 mM)
resolution cutoff (Å)	2.2	2.1	2.1	2.1	2.2
*I*2 unit cell [*a*, *b*, *c* (Å)]	196.3, 127.2, 133.8	196.2, 127.1, 133.7	196.9, 127.8, 134.4	195.7, 128.0, 134.2	196.1, 128.3, 134.5
*I*2 unit cell β angle (deg)	97.6	97.7	97.8	97.8	97.7
total observations (unique)	710 887[a] (150,371)	341 758 (154 926)	464 372 (161 912)	420 547 (169 385)	341 076 (144 344)
R_{merge}	0.102[a,b] (0.0675)[a,c]	0.058[b] (0.073)[c]	0.063[b] (0.101)[c]	0.071[b] (0.115)[c]	0.065[b] (0.092)[c]
$R_{isomorphous}$ to native[d]	0.171	0.159	0.185	0.269	0.262
fraction of data (resolution shell)	0.963[a] (10−2.2 Å) 0.892 (2.4−2.2 Å)	0.854 (10−2.1 Å) 0.577 (2.3−2.1 Å)	0.880 (10−2.1 Å) 0.514 (2.3−2.1 Å)	0.942 (10−2.1 Å) 0.854 (2.3−2.1 Å)	0.912 (10−2.2 Å) 0.832 (2.4−2.2 Å)
average intensity [$I/\sigma(I)$]	(10−2.2 Å)[a] 10.3	(10−2.1 Å) 9.6	(10−2.1 Å) 10.1	(10−2.1 Å) 8.15	(10−2.2 Å) 8.41
model refinement[e]					
reflections ($F \geq 1.0\sigma$)[e]	116 449	123 352	124 934	123 309	113 157
R-factor[f]	(6.0 −2.2 Å) 0.165 (2.4−2.2 Å) 0.212	(6.0 −2.1 Å) 0.173 (2.3−2.1 Å) 0.230	(6.0 −2.1 Å) 0.173 (2.2−2.1 Å) 0.238	(6.0 −2.1 Å) 0.184 (2.3−2.1 Å) 0.262	(6.0 −2.2 Å) 0.171 (2.4−2.2 Å) 0.234
rms deviation from ideal					
23 symmetry (Å)	0.158	0.187	0.159	0.202	0.18
bond distances (Å)	0.015	0.016	0.017	0.018	0.014
bond angles	3.0	3.2	3.1	3.1	2.9
number of non-H protein atoms	20 628	20 562	20 562	20 550	20 550
number of solvent O atoms	1392	1416	1452	1410	1416
ligands per asymmetric unit	12	6	6	6 INO and 6 CN	6 NNO and 6 CN
mean B values (Å^2)					
α-subunit, β-subunit, solvent	25.4, 19.0, 20.4	29.3, 23.5, 24.6	24.7, 18.1, 19.7	26.1, 19.4, 20.9	26.2, 19.7, 21.1
ligand (Å^2)	17.4 (17.5)[g]	23.9	19.6	19.5 (INO), 17.2 (CN)	19.1 (NNO), 17.7 (CN)

[a] Data combined from two crystals. [b] Weighted $R_{merge} = [\sum_{hkl}\sum_i[(I_i - \langle I\rangle_i G_i)/\sigma_i\}^2/\sum_{hkl}\sum_i(I_i/\sigma_i)^2]^{1/2}$. [c] Absolute $R_{merge} = \sum_{hkl}\sum_i |I_i - \langle I\rangle_i G_i|/\sum_{hkl}\sum_i I_i$, where, for observation *i* of reflection *hkl*, I_i is the observed intensity, $\langle I\rangle_i$ is its mean intensity, G_i is the scaling function applied, and σ_i is the standard deviation. [d] $R_{isomorphous} = \sum_{hkl}|F_{complex} - F_{native}|/\sum_{hkl}F_{native}$, where $F_{complex}$ and F_{native} are the structure factors for the 3,4-PCD complexes and 3,4-PCD as isolated, respectively. [e] Reflections between 6.0 Å and the resolution limit. [f] *R*-factor $= \sum_{hkl}|F_o - F_c|/\sum_{hkl}F_c$. [g] Average *B* value of the PCA molecules bound in the 3-fold binding site (Orville et al., 1997).

species. Presumably, this stability is due to the fact that INO and NNO bind to 3,4-PCD with much higher affinity than PCA. Consequently, the 3,4-PCD·INO·CN and 3,4-PCD·NNO·CN ternary complexes are ideally suited for crystallographic analysis.

In the present study, we report the crystal structures of the anaerobic 3,4-PCD·PCA complex, aerobic complexes formed with INO or NNO, and the ternary 3,4-PCD·INO·CN and 3,4-PCD·NNO·CN complexes. These data provide unambiguous structural evidence for (i) substrate chelation in a unique binding orientation, (ii) displacement of an endogenous Fe^{3+} ligand, (iii) dynamic expansion of the Fe^{3+} coordination sphere, and (iv) creation of a new binding pocket for small O_2-like molecules immediately adjacent to the site of oxygen insertion into the substrate ring. These results strongly support the salient aspects of the proposed mechanism and, together with the monohydroxy inhibitor binding studies reported in the preceding paper (Orville et al., 1997), support a logical progression of substrate reorientations in the active site that produce a form of the substrate that can be attacked by molecular oxygen. The novel mechanistic insights described here are likely to apply to other intradiol-cleaving dioxygenases, and perhaps to metalloenzyme catalysis in general.

MATERIALS AND METHODS

3,4-PCD was isolated from *P. putida*[3] grown on *p*-hydroxybenzoate and crystallized by vapor diffusion in hanging drops as previously described (Que et al., 1976; Ohlendorf et al., 1994). INO and NNO were synthesized as described by Whittaker and Lipscomb (1984b). Stock solutions of PCA, NNO, or INO at the concentrations indicated in Table 1 were made with the mother liquor obtained from the crystallization well, and the pH was adjusted to 8.4 by the addition of 1 equiv of NaOH. Stock solutions of NaCN (1 M) were prepared in a similar fashion, but H_2SO_4 was added to maintain a pH of approximately 8.4. The binary INO or NNO complexes were formed by gradually replacing the mother liquor with the analog stock solution in three steps (1:10, 1:1, final) followed by incubation at 23 °C for 5−12 h. The ternary 3,4-PCD·INO·CN and 3,4-PCD·NNO·CN complexes were formed by addition of NaCN (200 mM final concentration in one step) to previously formed binary complexes (20 mM INO or NNO). Data collection on the ternary complexes proceeded within 30 min of NaCN addition.

Two anaerobic PCA complexes were formed in separate 1.5 mm glass capillaries within a small anaerobic chamber. The 3,4-PCD crystals were equilibrated for 1 h with Ar that had been passed over a BASF Cu catalyst to remove traces of O_2. Anaerobic mother liquor containing 70 mM PCA (pH ∼8.4) was then injected into the capillaries to cover the crystal and incubated for an additional 1 h. After the crystal was dried, the capillary was sealed with epoxy prior to removing it from the chamber. The anaerobic conditions inside the sealed capillaries appeared to be maintained since the PCA stock solutions turned brown within minutes upon exposure to air whereas the same PCA solution sealed inside the capillaries remained colorless for months.

The X-ray diffraction data were collected at approximately 23 °C as previously reported (Ohlendorf et al., 1994; Orville et al., 1997). Data collection and model refinement statistics are reported in Table 1 for the *I*2 unit cell which are all isomorphous ($a = 196.2 \pm 0.4$ Å, $b = 127.7 \pm 0.5$ Å, $c = 134.1 \pm 0.4$ Å, and $\beta = 97.7 \pm 0.08°$). Atomic models

[3] American Type Culture Collection (ATCC) 23975, previously classified as *Pseudomonas aeruginosa*.

Table 2: Averaged *B*-Factor and Occupancy for Two Orientations of INO and NNO[a]

	INO up[b]		INO down[c]			NNO up[d]		NNO down[e]	
atom[f]	*B* (Å^2)	*Q*	*B* (Å^2)	*Q*	atom[f]	*B* (Å^2)	*Q*	*B* (Å^2)	*Q*
C4 (C1)	23.60 (0.04)	0.76 (0.15)	23.53 (0.05)	0.73 (0.10)	C3 (C1)	21.22 (0.04)	0.97 (0.08)	21.13 (0.06)	0.93 (0.10)
C3 (C2)	23.68 (0.06)	0.97 (0.08)	23.69 (0.06)	0.83 (0.08)	C2 (C2)	20.54 (0.08)	1.00 (0.00)	20.54 (0.03)	1.00 (0.00)
C2 (C3)	23.71 (0.02)	0.47 (0.10)	23.63 (0.01)	0.90 (0.11)	N1 (C3)	20.18 (0.02)	0.50 (0.17)	19.39 (0.13)	0.97 (0.08)
N1 (C4)	22.73 (0.05)	0.97 (0.08)	23.33 (0.04)	0.53 (0.10)	C6 (C4)	19.21 (0.07)	0.97 (0.08)	19.42 (0.03)	0.47 (0.24)
C6 (C5)	23.22 (0.03)	0.80 (0.13)	23.36 (0.02)	0.53 (0.16)	C5 (C5)	19.98 (0.02)	0.40 (0.13)	19.90 (0.08)	0.87 (0.16)
C5 (C6)	23.57 (0.01)	0.30 (0.17)	23.47 (0.04)	0.83 (0.20)	C4 (C6)	20.80 (0.02)	0.73 (0.21)	20.35 (0.08)	1.00 (0.00)
C7	23.56 (0.03)	0.87 (0.10)	23.49 (0.03)	0.87 (0.10)	C7	21.57 (0.05)	0.97 (0.08)	20.33 (0.07)	0.93 (0.10)
O1	24.16 (0.07)	0.77 (0.08)	23.54 (0.07)	0.90 (0.17)	O1	22.44 (0.03)	0.53 (0.10)	22.65 (0.13)	0.93 (0.10)
O2	23.41 (0.06)	0.90 (0.17)	23.57 (0.08)	0.80 (0.13)	O2	21.61 (0.05)	0.47 (0.16)	22.86 (0.21)	1.00 (0.00)
O3	24.34 (0.05)	0.67 (0.10)	23.18 (0.11)	0.93 (0.10)	O3	20.67 (0.05)	0.57 (0.08)	18.77 (0.21)	0.93 (0.10)
O4	22.35 (0.05)	0.40 (0.13)	23.05 (0.07)	0.57 (0.15)	O4	16.91 (0.25)	1.00 (0.00)	17.91 (0.10)	0.67 (0.10)
mean	23.48	0.72	23.44	0.77		20.47	0.74	20.3	0.88

[a] Average of the six active sites per asymmetric unit; 1 σ error is indicated in parentheses. [b] The INO orientation in which O3 coordinates the iron *trans* to His462$^{N\epsilon 2}$ after 10 cycles of refinement. [c] The INO orientation in which O3 coordinates the iron *trans* to Tyr408$^{O\eta}$ after 11 cycles of refinement. [d] The NNO orientation in which O3 coordinates the iron *trans* to His462$^{N\epsilon 2}$ after 17 cycles of refinement. [e] The NNO orientation in which O3 coordinates the iron *trans* to Tyr408$^{O\eta}$ after 16 cycles of refinement. [f] Atom names in parentheses corresponding to PCA are shown for reference (see Scheme 1).

for PCA, INO, NNO, and CN^- were built using the InsightII software package (Biosym Corp., La Jolla, CA). The Discover routine was also used to build an energy-minimized model of the proposed peroxy intermediate. The atomic labeling for the substrate and analogs is shown in Scheme 1, where OH3 or OH4 and O3 or O4 indicate neutral and ionic catecholic oxygen atoms, respectively. In addition, the phenolic oxygen atoms of tyrosine residues in the ionized or neutral state are indicated by Oη and OH atom names, respectively. X-ray reflections between 6 Å and the resolution limit and structure factors of $\geq 1\sigma$ were used to refine the atomic models (Ohlendorf et al., 1994; Orville et al., 1997) with PROLSQ (Hendrickson & Konnert, 1980; Hendrickson, 1985) on a Cray Y-MP supercomputer. The version of PROLSQ was modified so that the thermal factors for all hydrogen-bonded partners were restrained together. PCA, INO, and NNO were restrained to be planar, but all bond distances between the Fe^{3+} and coordinating atoms were not restrained during refinement. The final models are within error of other protein transition metal bond distances (Glusker, 1991), and the stereochemical quality of the refined structures was assessed with PROCHECK (Laskowski et al., 1993) and WHAT_CHECK (Hooft et al., 1996). The starting model for each complex was derived from the refined 3,4-PCD uncomplexed structure (PDB reference code 2PCD; Ohlendorf et al., 1994) from which all the active site solvent molecules had been removed, and the axial tyrosine (Tyr447) was either replaced with an alanine or rotated into the alternative position indicated by the 6-fold averaged initial difference Fourier maps produced as previously described (Orville et al., 1997).

Several refinement trials were performed to validate the orientation of PCA, INO, and NNO within the active site. For example, atomic models that differed only in the orientation of INO or NNO within the active site were refined against their respective data sets. In one model, O3 and O4 from INO (or NNO) coordinated the Fe^{3+} from axial and equatorial sites, respectively (the "up" orientation). In another model, the substrate analog was flipped approximately 180° to yield O3 and O4 atoms in equatorial and axial sites, respectively (the "down" orientation). During the refinement, the occupancy or thermal factors for the individual atoms in INO (or NNO), the Fe^{3+}, and all the solvent molecules were refined on alternating passes. These refinement trials yielded comparable *R*-factors; however, the down orientation models yielded lower *B*-factors, higher occupancies, and cleaner $|F_o| - |F_c|$ difference maps than their flipped counterparts (Table 2).

Table 3: *B*-Factors and Occupancy for the Sixth Ligand in Models for the *N*-Oxide Complexes[a]

complex	ligand *trans* to H460$^{N\epsilon 2}$	atom	*B* (Å^2)[b]	*Q*[b]
3,4-PCD·INO	solvent	O	22.15 (0.14)	0.733 (0.10)
	cyanide	C	18.28 (0.18)	1
		N[c]	20.19 (1.5)	1
3,4-PCD·NNO	solvent	O	16.62 (0.06)	1
3,4-PCD·INO·CN	solvent	O	19.25 (0.10)	1
	cyanide	C	16.63 (0.10)	1
		N	17.86 (0.24)	1
3,4-PCD·NNO·CN	cyanide	C	17.39 (0.08)	1
		N	18.00 (0.12)	1

[a] Models with either a solvent molecule or the carbon atom of cyanide bound *trans* to His460Nϵ2 were refined against the indicated data set until convergence. [b] Averaged from the six active sties per asymmetric unit. [c] There was a significant (more than 5σ) negative $|F_o| - |F_c|$ feature associated with this atom.

Several atomic models were also refined to validate ligands coordinating the iron *trans* to His460$^{N\epsilon 2}$. This was important to test the ability to differentiate between (i) an unoccupied coordination site, (ii) a site containing a single atom, and (iii) a site coordinating a diatomic molecule. For example, models without a ligand, a one-atom ligand (a solvent molecule), or a two-atom ligand (a CN^- molecule) in the coordination site were refined against the 3,4-PCD·INO and 3,4-PCD·INO·CN data sets (Table 3). On the basis of these types of refinement trials, the data from the 3,4-PCD·PCA, 3,4-PCD·INO, and 3,4-PCD·NNO complexes are sufficient to discriminate between an unoccupied site, a one-atom ligand, or a two-atom ligand in the site opposite His460$^{N\epsilon 2}$. However, Fourier maps of comparable quality were obtained from both ternary complexes (3,4-PCD·INO·CN or 3,4-PCD·NNO·CN) refined with either a CN^- molecule or a solvent molecule located in a position analogous to the center of the CN^-. This result notwithstanding, several observations compel us to favor the structure for the ternary complexes that include the CN^- rather than a solvent molecule (see below).

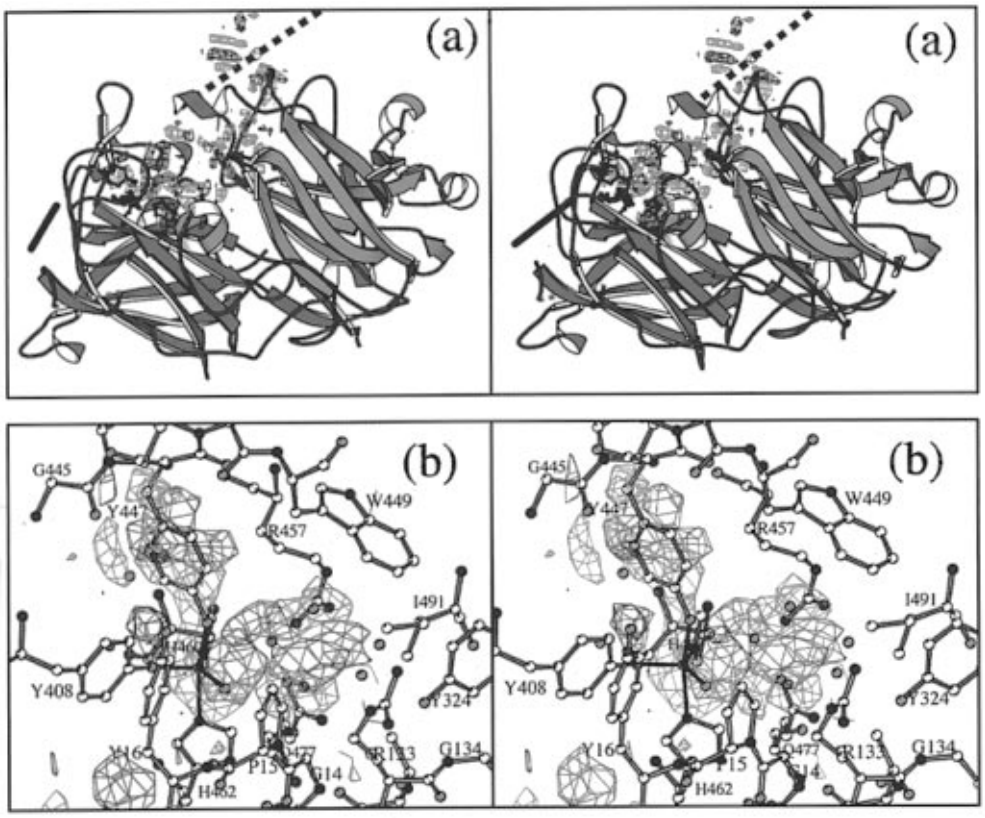

FIGURE 1: Difference Fourier maps for the 3,4-PCD·PCA complex minus 3,4-PCD calculated with $|F_{P\cdot PCA}| - |F_P|$ amplitudes for data between 5 and 2.15 Å with phases from the refined structure of 3,4-PCD as isolated. (a) Divergent stereo view of the 6-fold averaged difference maps contoured at $+5\sigma$ (blue) and -5σ (red) superimposed upon protomer A of uncomplexed 3,4-PCD. The C^{α} ribbon traces are shown for the α- and β-subunits in red and green, respectively. A 2-fold and 3-fold symmetry axis is indicated by the black solid and dashed lines, respectively. (b) Stereoview in the active site region of the averaged $+4\sigma$ (blue) and -4σ (red) difference Fourier maps superimposed on the uncomplexed enzyme structure. Bonds for the α- and β-subunits are shown in red and green, respectively; carbon, oxygen, and nitrogen atoms are white, red, and blue, respectively.

The overall structures of the 3,4-PCD complexes were very similar to those of uncomplexed 3,4-PCD and the monohydroxy inhibitor complexes reported in the previous paper (Orville et al., 1997). One exception is that addition of NaCN to the preformed binary 3,4-PCD·INO or 3,4-PCD·NNO complex appears to eliminate the β-mercaptoethanol modification at $Cys429^{S\gamma}$ observed for the other complexes and uncomplexed enzyme. In addition, a precipitate was formed in the mother liquor of the ternary complexes but did not affect the diffraction of the complexes.

Figures 1 and 6a,b were made with MINIMAGE (Arnez, 1994) and MOLSCRIPT (Karulis, 1991). Figures 4, 6c, and 7 were prepared with MOLSCRIPT (Karulis, 1991). Figures 3 and 5 were prepared with MIDAS+ [Ferrin et al., 1988; from the Computer Graphics Laboratory of the University of California at San Francisco (supported by NIH Grant RR-01081)].

RESULTS

Anaerobic 3,4-PCD·PCA Complex. Formation of anaerobic substrate complexes changes the burgundy-red-colored crystals of 3,4-PCD as isolated to a dark blue color that is characteristic of the substrate complex formed in solution. The 6-fold averaged $|F_{P\cdot PCA}| - |F_P|$ Fourier difference maps (Figure 1) indicate that several structural alterations occur upon substrate binding. First, a series of positional shifts extends approximately 20 Å from the active site along the α-subunit−β-subunit interfaces. Similar structural perturbations are also observed in the other complexes in this report and in the competitive inhibitor complexes in the previous paper [e.g. Figure 3 in Orville et al. (1997)]. Second, the $|F_{P\cdot PCA}| - |F_P|$ and $2|F_{P\cdot PCA}| - |F_P|$ electron density maps clearly indicate that a PCA molecule binds in each active site. However, these maps also show that three PCA molecules bind around the local 3-fold symmetry axes in orientations that are virtually indistinguishable from those of the 3-halo-4-hydroxybenzoate inhibitors described in the preceding paper. Third, as shown in Figure 1b, PCA binding within the active site causes either dissociation or positional shifts of most of the active site solvent molecules observed in the structure of 3,4-PCD as isolated. Finally and most interestingly, the $\pm 4\sigma$ initial $|F_{P\cdot PCA}| - |F_P|$ difference Fourier maps (Figure 1b) clearly suggest that both the axial tyrosinate (Tyr447) and Wat827 dissociate from the Fe^{3+} upon PCA binding.

There are no large positional differences in the main chain atoms between the 3,4-PCD·PCA complex and the other complexes in this report. The rms difference between the uncomplexed 3,4-PCD structure and the refined 3,4-PCD·PCA complex is approximately 0.4 Å when averaged over all the main chain atoms in one protomer. Figure 2 plots the positional shifts averaged over either the main chain or all atoms per residue. The region with the largest differences results from positional shifts in both the main chain and side chain atoms of residues 23−28 and 95−102 in the α-subunit (Ohlendorf et al., 1994). This area has approximately the

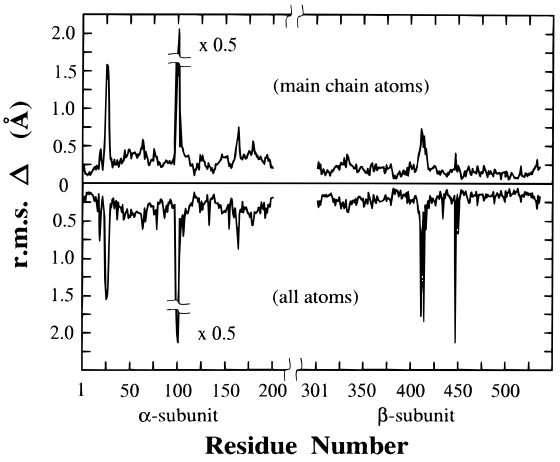

FIGURE 2: Positional shifts in the main chain and side chain for the 3,4-PCD·PCA complex relative to the structure of 3,4-PCD as isolated. The rms differences were averaged over the backbone atoms or all the atoms per residue as indicated in the panels. Note that the differences centered around residue 99 have been reduced by a factor of 2.

same structure in all the complexes of this report and the competitive inhibitor complexes of the preceding report (Orville et al., 1997). In contrast to the main chain conformational changes that occur in the α-subunit, the largest alterations in the β-subunit structure are restricted to shifts in the side chain orientation of Tyr447, Lys411, and Arg414. The latter two differences were also observed in the competitive inhibitor complexes [see Figure 3 of Orville et al. (1997)], but the alteration to Tyr447 was only observed in the substrate and substrate analog complexes reported here.

The 6-fold averaged $2|F_o| - |F_c|$ electron density maps in the region of the active site for each of the complexes unambiguously show that three iron ligands, $Tyr408^{O\eta}$, $His460^{N\epsilon 2}$, and $His462^{N\epsilon 2}$, remain coordinated, whereas Tyr447 is in an alternative orientation (Figure 3). There is planar electron density encompassing the aromatic ring and the carboxylate group of PCA, INO, or NNO in each complex. However, the C4, C5, and O4 atoms in PCA and analogous atoms in INO or NNO had slightly less $2|F_o| - |F_c|$ electron density and larger *B*-values than the other atoms of the substrate or analogs (Table 2). Nevertheless, the $2|F_o| - |F_c|$ density connecting the substrate or substrate analog to the Fe^{3+} is obviously stronger than the analogous region for the monodentate $Tyr408^{O\eta}$ ligand. Therefore, chelated Fe^{3+} complexes are supported by the overall electron density.

Views of the active site region for the anaerobic 3,4-PCD·PCA structure are shown in Figure 4 and compared with the structures of 3,4-PCD as isolated (Ohlendorf et al., 1994) and the 3,4-PCD·FHB complex (Orville et al., 1997). Hydrophobic interactions between PCA and Gly14, Pro15, Trp449, and Ile491 align the plane of the aromatic ring of PCA approximately parallel with the axial iron ligand axis. In addition, strong hydrogen bonds are formed between PCA^{O1} and $Tyr324^{OH}$ at the back of the active site cavity and between PCA^{O3} and $Arg457^{N\eta 1}$ near the iron. These substrate−active site interactions restrict the orientation of the aromatic ring of PCA and consequently set up a steric conflict between PCA^{O4} and $Tyr447^{O\eta}$ in the uncomplexed structure (Figure 4a). Rotation of the Tyr447 X_1 ($N-C^{\alpha}-C^{\beta}-C^{\gamma}$) torsion bond angle from 59° in the uncomplexed structure to 171° in the PCA complex removes the steric clash. The alternative orientation of Tyr447 is stabilized through hydrogen bonds to $Tyr16^{OH}$ and $Asp413^{O\delta 1}$ (Figure 4b). Formation of the PCA·Fe^{3+} chelated complex shifts the iron approximately 0.4 Å toward PCA relative to the uncomplexed structure. There is no electron density in the 3,4-PCD·PCA complex to indicate a coordinating molecule in the iron site opposite $His460^{N\epsilon 2}$; we therefore view this as an open coordination site.

The comparison of the 3,4-PCD·FHB and 3,4-PCD·PCA complexes reveals several interesting observations (Figure 4a). Although the C3-halide in FHB is comparable in steric bulk to the C3-phenolate group of PCA, the halide is unable to coordinate the iron and consequently FHB binds to optimize hydrogen bonds with $Arg457^{N\eta 1}$ and $Gln477^{N\epsilon 2}$. In contrast, the $2|F_o| - |F_c|$ electron density for the 3,4-PCD·PCA complex is most consistent with the PCA^{O3} group coordinating the iron to form a chelate complex. The orientation observed for the PCA molecule is related to that of FHB via an approximately 18 ± 3° in-plane pivot about C1. The binding of FHB requires only minor changes in the overall structure of the resting enzyme. The main chain atoms for the 3,4-PCD·PCA and 3,4-PCD·FHB complexes superimpose with an rms deviation of 0.12 Å, and the Fe^{3+} atom in the 3,4-PCD·FHB complex is shifted 0.2 Å relative to both uncomplexed 3,4-PCD and the 3,4-PCD·PCA complex. This suggests that the FHB complex partially shifts the enzyme into the conformation of the 3,4-PCD·PCA complex, but chelation of the iron with the concomitant dissociation of Tyr447 is required to fully manifest the conformational change.

Since there are six active sites per asymmetric unit, we averaged the bonding parameters for the iron center in each active site (Table 4). The resulting statistical uncertainty can be used as an independent measure of the structural flexibility within the active site. For example, the bond distances for the three endogenous Fe^{3+} ligands of the 3,4-PCD·PCA complex have lower standard deviations than either of the $Fe^{3+}-PCA^{catecholic-O}$ bonds, suggesting that they have less variability. The average $Fe^{3+}-PCA^{O4}$ bond distance is 2.16 ± 0.14 Å, whereas the average equatorial $Fe^{3+}-PCA^{O3}$ bond distance is 2.41 ± 0.28 Å. Therefore, the asymmetric PCA·Fe^{3+} complex[4] has the shorter bond opposite $His462^{N\epsilon 2}$ and the longer bond opposite $Tyr408^{O\eta}$. The Fe^{3+} is also approximately 0.8 Å out of the plane of the PCA ring (Figure 4b and Table 4). Several active site residues appear to prevent the formation of a symmetric Fe^{3+}·catecholate complex. For example, the position of Pro15 and Ile491 disrupts the formation of a planar, five-membered ring in the chelated Fe^{3+}·PCA complex. The hydrogen bond between $Arg457^{N\eta 1}$ and PCA^{O3} and the potential for *trans* ligand influences also enhance the asymmetry of the chelate Fe^{3+}·PCA complex.

Figure 5 shows the solvent accessible surface area for residues within the active site of the 3,4-PCD·PCA complex. The C6, O1, C3, and C4 atoms of PCA each have solvent accessible surfaces, but only 20% of the total PCA surface area is exposed. The surface areas on the C6 and O1 atoms

[4] The crystal structure and complementary resonance Raman studies for the 3,4-PCD·HPCA complex also show that HPCA (an alternative substrate) asymmetrically chelates the iron (Elgren, T. E., Orville, A. M., Kelly, K. A., Lipscomb, J. D., Ohlendorf, D. H., & Que, L., Jr., in press). Subtle structural differences between the PCA orientation relative to that observed for HPCA may explain the more efficient oxidation of PCA relative to that of HPCA by 3,4-PCD.

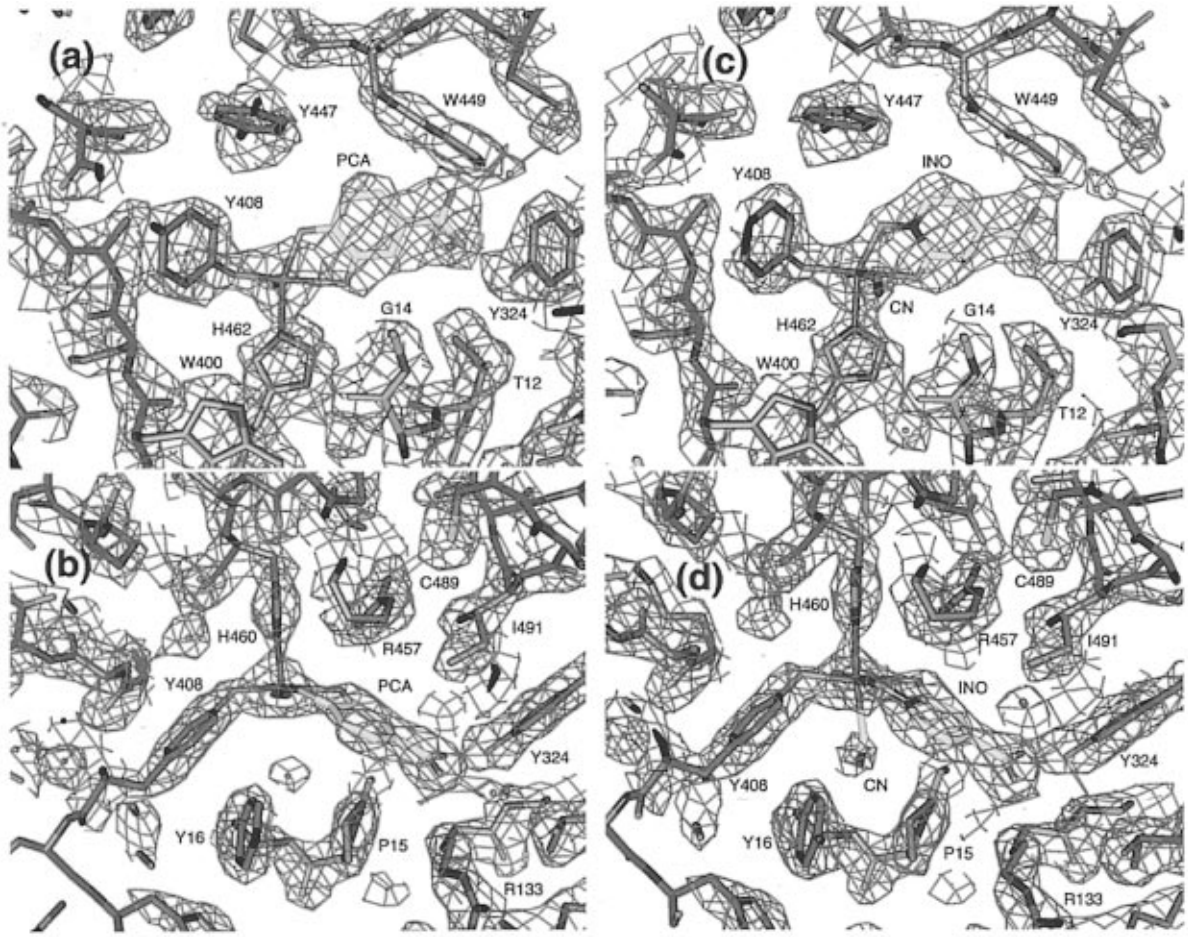

FIGURE 3: Examples of 6-fold averaged $2|F_o| - |F_c|$ electron density maps calculated with data between 6 and 2.2 Å resolution contoured at 1.5σ superimposed on their respective atomic models. Approximately perpendicular views in the active site region of the 3,4-PCD·PCA complex (a and b) or the 3,4-PCD·INO·CN complex (c and d). Carbon atoms are colored red, green, gray, or yellow for α- or β-subunit backbone atoms, side chain atoms, or PCA and INO atoms, respectively. N, O, and Fe^{3+} atoms are colored blue, red, and magenta, respectively.

are exposed to bulk solvent, whereas the area of the C3 and C4 atoms, which is the site of ring cleavage, is adjacent to a small, spherical cavity that is sequestered from bulk solvent. Because of the size and location of this cavity, we speculate that this is the O_2 binding site. The top of the cavity is formed by Tyr447 in the alternative position, while the bottom is comprised of Ala13, Val17, Trp400, and His462. The equatorial walls of the cavity are formed by residues Gly14, Pro15, Tyr16, and Tyr408 and PCA. On the other side of the Fe^{3+} opposite PCA, another cavity, which is also inaccessible to bulk solvent, is lined by Ala402, His460, and Tyr408. Both cavities contain solvent molecules that participate in several hydrogen bonds and are well-ordered as indicated by their low thermal parameters (ranging from ~10 to 15 Å^2) and full occupancy. Of particular interest is Wat606, which is hydrogen bonded in tetrahedral geometry to $Trp400^{N\epsilon1}$, $Tyr16^{N}$, and $Ala12^{O}$ and probably reduces the effective volume of the putative O_2 cavity. Moreover, the two donating hydrogen bonds to Wat606 ($Trp400^{N\epsilon1}$ and $Tyr16^{N}$) and a single accepting hydrogen bond ($Ala12^{O}$) may orient Wat606 so that a proton with its $\delta+$ charge points toward the O_2 site and any reaction intermediates that form near this position.

Structures of the Binary 3,4-PCD·INO/NNO and Ternary 3,4-PCD·INO/NNO·CN Complexes. Both INO ($K_{D\ overall} = 0.06\ \mu M$) and NNO ($K_{D\ overall} = 0.20\ \mu M$) form high-affinity dead end complexes with the enzyme (Lipscomb et al., 1982; May et al., 1982; Whittaker & Lipscomb, 1984b). The aerobic addition of INO or NNO to 3,4-PCD crystals rapidly bleaches the color to a pale yellow that is indistinguishable from the color of the solution complex. Subsequent addition of NaCN to the final binary INO or NNO complex causes the yellow crystals to turn purple, as observed for complexes in solution (Whittaker & Lipscomb, 1984a). These four complexes exhibit optical properties dramatically different than those of the resting 3,4-PCD or the 3,4-PCD·PCA complex and are thought to stabilize the enzyme in conformations that mimic intermediates beyond the anaerobic PCA complex in the proposed reaction pathway.

The orientation and Fe^{3+} coordination distances of INO and NNO in the binary and ternary enzyme complexes are very similar to that observed for PCA (Tables 2 and 4). However, the presence of a sixth coordinating ligand in each complex differentiates them from PCA (Figure 6). Since this coordination site projects into the putative O_2 cavity, it warrants careful attention. The $2|F_o| - |F_c|$ and $|F_o| - |F_c|$ omit electron density maps (Figure 6a) as well as the *B*-factors for the sixth iron ligand (Table 3) of the INO and NNO binary complexes are each most consistent with a solvent molecule coordinated to the iron. The solvent molecule forms a hydrogen bond with Wat606. These structures are in accord with previous EPR results that detected ^{17}O-enriched solvent bound to the iron in the final INO and NNO complexes (Whittaker & Lipscomb, 1984a).

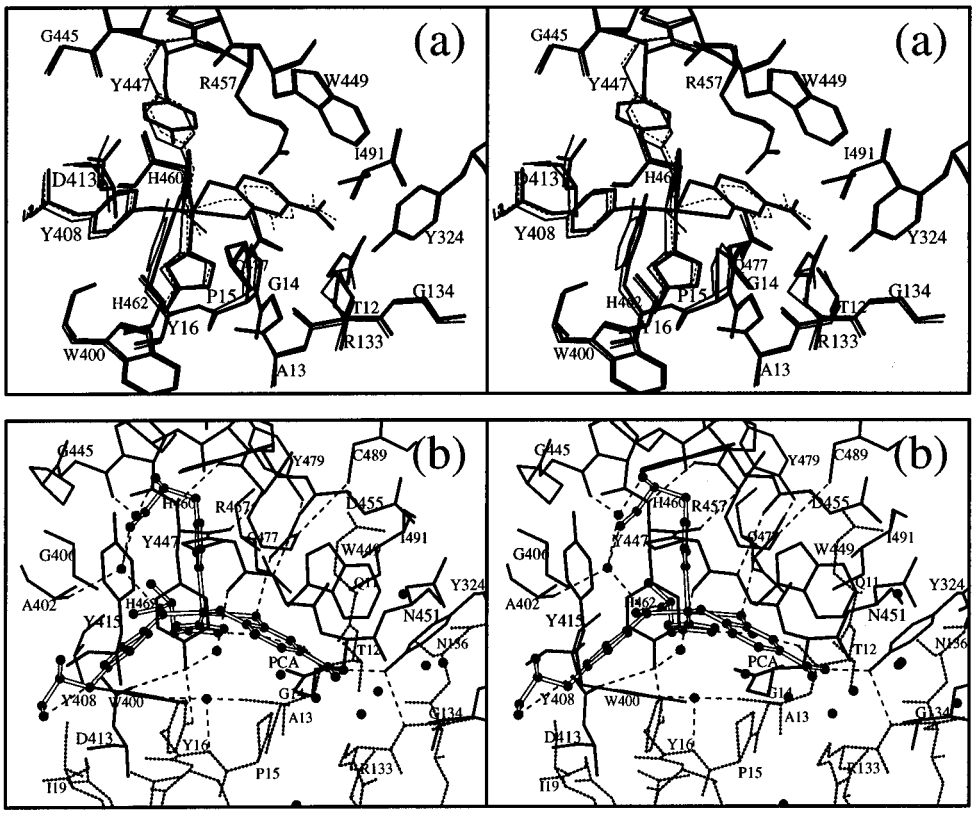

FIGURE 4: Divergent stereoviews of the structure for the binary 3,4-PCD·PCA complex. (a) A view approximately parallel to the Fe^{3+} equatorial plane for the 3,4-PCD·PCA complex (thick solid lines) and a superposition of the structure of uncomplexed 3,4-PCD (thin solid lines) and the 3,4-PCD·FHB complex (thin dashed line; Orville et al., 1997). (b) An approximately perpendicular view of the 3,4-PCD·PCA complex highlights the relative orientation of Tyr447, PCA, and the open coordination site opposite $His460^{N\epsilon 2}$. Hydrogen bonds are indicated with dashed lines.

Table 4: Averaged Bond Distances[a] and Angles[b] for the Six Active Site Fe^{3+} Centers per Asymmetric Unit[c]

	PCA	INO	NNO	INO + NaCN	NNO + NaCN
$Tyr408^{O\eta}$−Fe distance (Å)	1.99 (0.04)	2.04 (0.07)	2.02 (0.10)	2.02 (0.11)	1.95 (0.06)
$His460^{N\epsilon 2}$−Fe distance (Å)	2.25 (0.06)	2.36 (0.11)	2.41 (0.05)	2.31 (0.12)	2.31 (0.08)
$His462^{N\epsilon 2}$−Fe distance (Å)	2.18 (0.05)	2.25 (0.09)	2.21 (0.09)	2.27 (0.08)	2.21 (0.04)
$subst^{O3}$−Fe[d] distance (Å)	2.41 (0.28)	2.44 (0.05)	2.43 (0.14)	2.43 (0.08)	2.36 (0.13)
$subst^{O4}$−Fe[e] distance (Å)	2.16 (0.14)	2.01 (0.13)	2.13 (0.09)	2.19 (0.13)	2.15 (0.06)
site C−Fe[f] distance (Å)	−	2.06 (0.11)	2.21 (0.10)	2.20 (0.14)	2.15 (0.17)
substrate plane−Fe distance (Å)	0.80 (0.02)	0.96 (0.02)	1.17 (0.04)	1.11 (0.02)	1.14 (0.03)
$Fe-CN^{C}-CN^{N}$ angle (deg)	−	−	−	144 (17)	156 (17)
$Tyr408^{O\eta}$−Fe−$His460^{N\epsilon 2}$ angle (deg)	90 (3)	86 (4)	85 (3)	90 (6)	89 (3)
$Tyr408^{O\eta}$−Fe−$His462^{N\epsilon 2}$ angle (deg)	96 (5)	97 (5)	98 (4)	98 (6)	98 (6)
$Tyr408^{O\eta}$−Fe−$subst^{O3}$ angle (deg)	171 (3)	173 (4)	170 (5)	172 (4)	173 (5)
$Tyr408^{O\eta}$−Fe−$subst^{O4}$ angle (deg)	103 (3)	105 (5)	105 (4)	107 (6)	105 (4)
$Tyr408^{O\eta}$−Fe−site C angle (deg)	−	100 (5)	103 (3)	100 (6)	102 (7)
$His460^{N\epsilon 2}$−Fe−$His462^{N\epsilon 2}$ angle (deg)	92 (5)	86 (4)	84 (4)	84 (5)	86 (4)
$His460^{N\epsilon 2}$−Fe−$subst^{O3}$ angle (deg)	99 (3)	92 (3)	87 (3)	88 (2)	87 (4)
$His460^{N\epsilon 2}$−Fe−$subst^{O4}$ angle (deg)	101 (4)	97 (4)	96 (5)	97 (4)	95 (5)
$His460^{N\epsilon 2}$−Fe−site C angle (deg)	−	170 (3)	169 (4)	162 (7)	164 (5)
$His462^{N\epsilon 2}$−Fe−$subst^{O3}$ angle (deg)	85 (3)	87 (3)	87 (6)	87 (4)	86 (3)
$His462^{N\epsilon 2}$−Fe−$subst^{O4}$ angle (deg)	157 (4)	157 (3)	157 (7)	155 (4)	157 (3)
$His462^{N\epsilon 2}$−Fe−site C angle (deg)	−	89 (4)	92 (5)	81 (6)	84 (3)
$subst^{O3}$−Fe−$subst^{O4}$ angle (deg)	75 (3)	71 (1)	70 (3)	69 (1)	71 (3)
$subst^{O3}$−Fe−site C angle (deg)	−	82 (2)	85 (5)	83 (2)	82 (4)
$subst^{O4}$−Fe−site C angle (deg)	−	86 (5)	85 (4)	94 (5)	90 (4)

[a] Estimated bond distance errors are ~0.25 Å on the basis of Luzzati (1952) analysis. [b] Estimated bond angle errors are ±3°. [c] The mean values (±1 σ error) of the six independent active sites per asymmetric unit are shown. [d] The C3-phenolic group of PCA and analogous substituents in INO and NNO (see Scheme 1). [e] The C4-phenolic group of PCA and analogous substituents in INO and NNO (see Scheme 1). [f] The iron coordination site opposite $His460^{N\epsilon 2}$ occupied by solvent in the INO and NNO complexes or by CN^- in the ternary complexes.

The ternary complexes formed with either analog and NaCN yield electron density maps that are most consistent with CN^- displacing the solvent molecule. This is particularly apparent in the $+5\sigma\,|F_o| - |F_c|$ omit difference map (Figure 6b) that yields an approximately 2-fold greater intensity than the analogous map for the binary complexes. In addition, the *B*-factors for both atoms of the cyanide ligand are lower than that obtained from a trial refinement with a solvent molecule replacing the cyanide (Table 3). As shown in Figure 6c, the distal end of the CN^- molecule is hydrogen bonded to

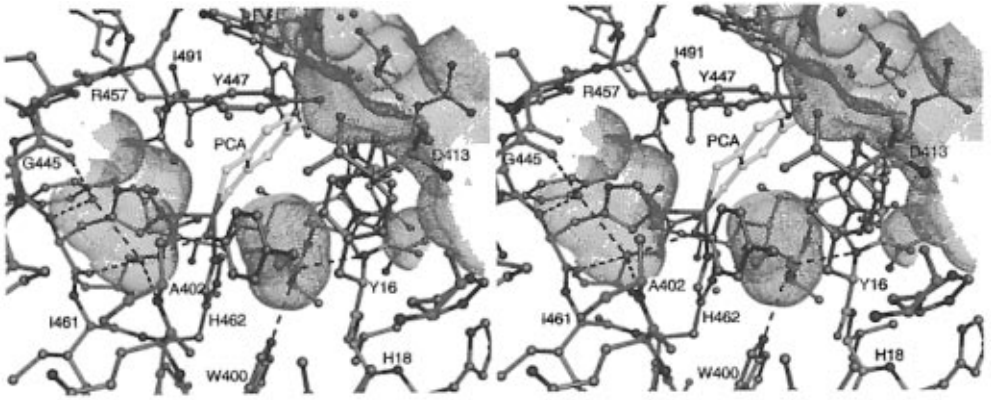

FIGURE 5: Divergent stereoview of the solvent-exposed surface area in the active site region of the 3,4-PCD·PCA complex. Solvent-exposed surfaces adjacent to PCA and α- and β-subunit residues are shown in yellow, red, and green dots, respectively. The C^{α} and C atoms from the α- and β-subunits are shown in red and green, respectively. The Fe^{3+}, O, N, and S atoms are shown in magenta, red, blue, and yellow, respectively. Hydrogen bonds are indicated by dashed lines.

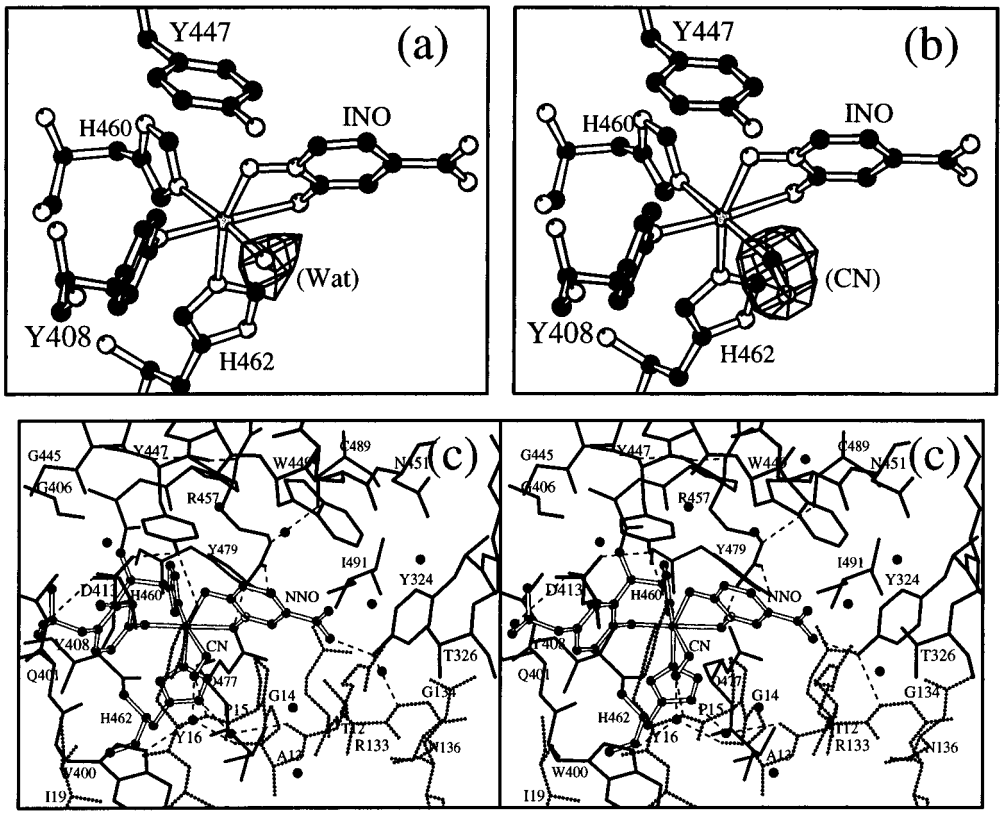

FIGURE 6: Structures of the binary and ternary complexes of 3,4-PCD with INO, NNO, and CN^- reveal ligands bound in the Fe^{3+} ligand site *trans* to $His460^{N\epsilon 2}$. (a) The 6-fold averaged, $+5\sigma\ |F_o| - |F_c|$ omit electron density (data between 6 and 2.1 Å) superimposed upon the final model for the 3,4-PCD·INO complex. The map was calculated with phases from the refined model in which the exogenous solvent had been omitted. (b) The 6-fold averaged $+5\sigma\ |F_o| - |F_c|$ omit electron density (data between 6 and 2.1 Å) calculated for the refined 3,4-PCD·INO·CN complex from which the CN^- ligand was omitted. (c) A divergent stereoview of the active site region in the 3,4-PCD·NNO·CN complex. Hydrogen bonds are indicated with dashed lines.

$Tyr16^N$ and Wat606 in the bottom of the O_2 cavity. These interactions may consequently produce the unusual nonlinear $Fe^{3+}-C\equiv N$ bond angle[5] of approximately 145° that is observed (Table 4). Such a nonlinear bond would likely reduce the orbital overlap between the iron and ^{13}CN greatly and is consistent with the absence of observable superhyperfine broadening in the 3,4-PCD·PCA·^{13}CN (Orville et al., 1989) and 3,4-PCD·INO·^{13}CN (A. M. Orville and J. D. Lipscomb, unpublished observation) complexes.

DISCUSSION

We show here that the process of substrate binding to 3,4-PCD results in a different orientation for substrate in the active site from what we reported for monohydroxy inhibitor complexes in the preceding paper (Orville et al., 1997). Past studies have shown that none of the inhibitors undergoes ring opening even at a very slow rate. Indeed, the presence of two vicinal phenolate groups is required for intradiol cleavage of any substrate for all known Fe^{3+}-containing

[5] The starting point for refining both ternary complexes was a 1.9 Å, linear $Fe^{3+}-C\equiv N$ complex in each active site. After refinement, the average $Fe^{3+}-C$ bond distance is about 2.2 Å with a 144 and 156° (±17°) $Fe^{3+}-C\equiv N$ bond angles (Table 4) for each complex. In the six independent active sites, the C atom (assumed to be the atom bound to the iron) is in a relatively consistent position while the N atom is more variable.

dioxygenases. The present studies make it clear that one reason for the requirement of the catecholate nucleus is the formation of the chelate complex which stabilizes the substrate in its unique binding orientation. In this orientation, four significant aspects of the reaction center are changed relative to the resting enzyme. First, the iron converts from trigonal bipyramidal to square pyramidal coordination geometry. Second, the substrate is bound as a dianion that is susceptible to electrophilic attack. Third, a cavity that can bind O_2-sized molecules is created in the appropriate position beside the carbon atom to be attacked on the substrate. Fourth, solvent is released from an iron coordination site which forms one side of the putative O_2 binding cavity, thereby opening a metal coordination site for use in the ensuing chemical reactions. The last three of these features are unique to the substrate complex. In the following paragraphs, the significance of these structural changes with respect to the detailed molecular mechanism of 3,4-PCD is discussed. Also, the significance of these results with respect to the reaction specificity of other dioxygenases and related non-heme Fe^{3+} enzymes is examined.

Mechanistic Insights from the Crystal Structures. The current mechanistic proposal for 3,4-PCD (Scheme 1) is based upon kinetic and spectroscopic results [reviewed in Lipscomb and Orville (1992)]. The structural data presented here and in the previous paper support this proposal, but they also allow a considerably more detailed hypothesis to be advanced. Figure 7 summarizes the active site structures of several complexes that seem to provide a reasonable description of the progression from initial substrate interaction with 3,4-PCD to the species from which O_2 attack occurs. The revised reaction mechanism based on these structures is presented in Figure 8.

The binding of substrates is thought to be very fast ($k_{on} > 1 \times 10^6\ M^{-1}\ s^{-1}$) and probably includes several intermediates on the basis of transient kinetic measurements of PCA and INO binding reactions (Fujisawa et al., 1971, 1972; Bull et al., 1981; Whittaker & Lipscomb, 1984b). In the preceding paper, it was suggested that the initial binding is directed by positive electrostatic fields emanating from the surface of the holoenzyme directly over each active site (Orville et al., 1997). Upon entering the active site, the PCA^{O4} group is proposed to coordinate the iron. The 3,4-PCD·IHB structure shown in Figure 7b is thought to mimic this initial 3,4-PCD·PCA intermediate and is remarkably similar to one of the PCA orientations predicted by computer docking experiments using the refined structure of 3,4-PCD as isolated (Ohlendorf et al., 1994). Since there is no other active site base, the hydroxide ligand (Figure 7a, Wat827) probably facilitates the deprotonation of PCA^{O4} ($pK_a \approx 8.8$; Smith & Martell, 1989) as we and others have previously proposed (Felton et al., 1984; True et al., 1990; Ohlendorf et al., 1994; Orville et al., 1997). In the 3,4-PCD·IHB complex, the C3-iodo group prevents the aromatic ring from binding deeper in the active site cavity and consequently mimics a weakly bound, early 3,4-PCD·PCA intermediate. PCA could rapidly shift to an orientation analogous to FHB in the 3,4-PCD·FHB complex (Figure 7c) as it penetrates deeper into the active site cavity to yield a second, more tightly bound intermediate. Solvent displaced as water in the previous step could presumably rebind in the new coordination site to yield an iron coordination sphere with octahedral symmetry. Rotation of the FHB-like intermediate about PCA^{C1} and concomitant dissociation of Tyr447 would readily yield the anaerobic 3,4-PCD·PCA complex (Figure 7d). We propose that the dissociation of Tyr447 results in the generation of a second active site base with a pK_a (>10) that is close to that of the PCA^{O3} ($pK_a \approx 11.7$; Smith & Martell, 1989) group. Deprotonation results in formation of the chelated dianionic 3,4-PCD·substrate complex indicated by previous spectroscopic results (Tyson, 1975; Lauffer & Que, 1982; Whittaker & Lipscomb, 1984b; Orville & Lipscomb, 1989).

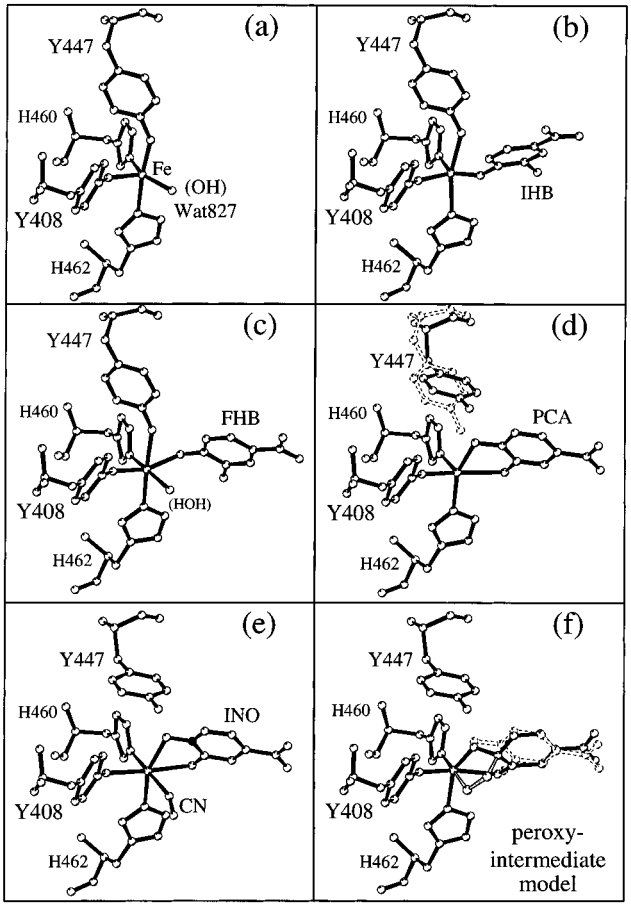

FIGURE 7: Iron coordination sphere in several 3,4-PCD complexes proposed to mimic intermediates of catalysis (see the text). The coordinating residues to the Fe^{3+} are shown for (a) 3,4-PCD as isolated (Ohlendorf et al., 1994), (b) the 3,4-PCD·IHB complex (Orville et al., 1997), (c) the 3,4-PCD·FHB complex (Orville et al., 1997), (d) the anaerobic 3,4-PCD·PCA complex (Tyr447 from the FHB complex is superimposed in dashed lines), (e) the ternary 3,4-PCD·INO·CN complex, and (f) an energy-minimized hypothetical model for the peroxy intermediate (PCA is superimposed in dashed lines).

Throughout this binding process, each of the proposed intermediates maintains charge neutrality at the metal center. This is accomplished by the deprotonation of the catecholate oxygens of PCA coincident with the dissociation of the solvent OH^- molecule as water and tyrosinate 447 as a neutral tyrosyl moiety. This not only produces substrate in the proper alignment for catalysis but also yields the dianionic chelated $PCA{\cdot}Fe^{3+}$ complex that we believe is necessary for electrophilic attack by O_2. Moreover, the presence of two active site bases ensures the generation of the dianionic $PCA{\cdot}Fe^{3+}$ complex over a wide pH range that matches the pH activity profile (pH 6.5 to >9.5) for 3,4-PCD (Fujisawa & Hayaishi, 1968). Finally, each of the proposed intermediates also progresses logically from lower-

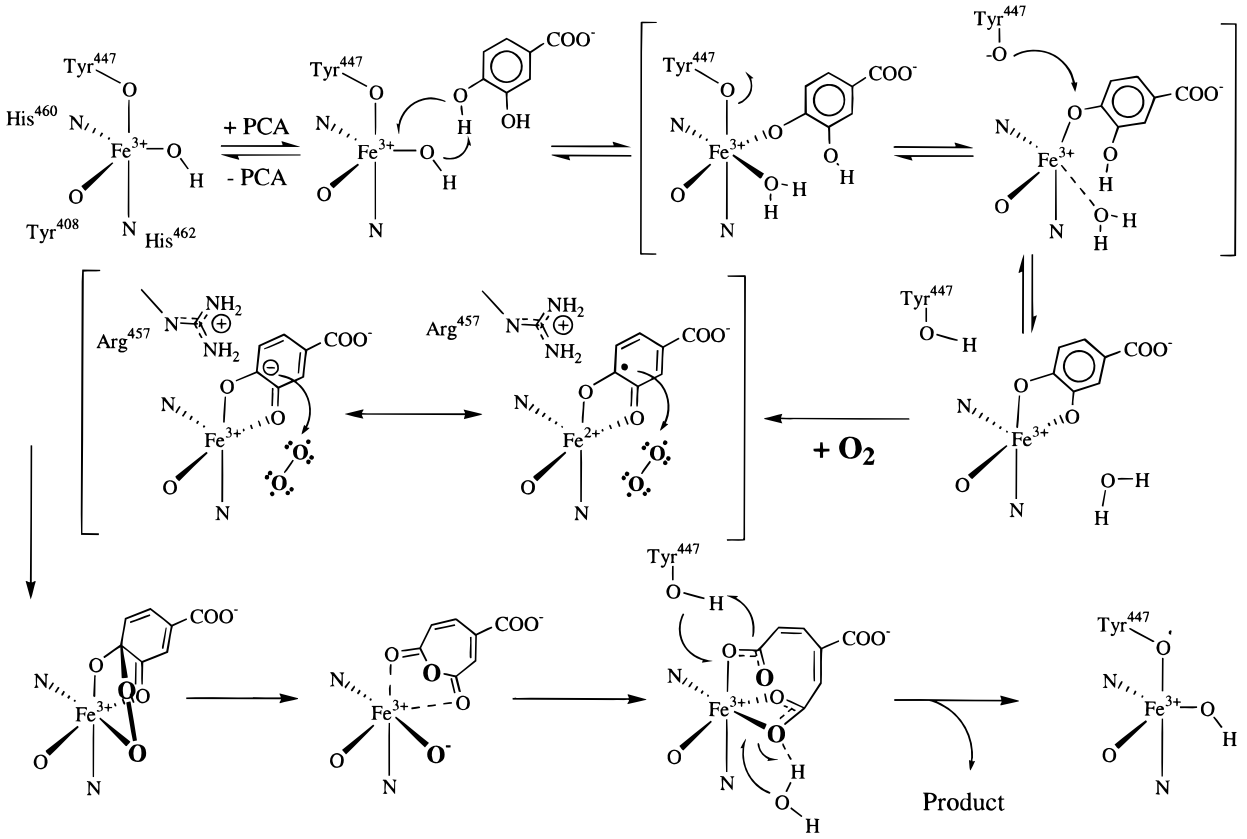

FIGURE 8: Reaction mechanism proposed for 3,4-PCD on the basis of kinetic, spectroscopic, and crystallographic data (see the text for the narrative).

to higher-affinity complexes, suggesting favorable changes in the free energy for the binding reaction.

Electrophilic attack of O_2 on the activated species of PCA to yield completely specific ring cleavage requires access of O_2 to the appropriate position of the substrate. Moreover, all of the kinetic studies to date indicate that O_2 interacts with the enzyme after substrate is bound. These aspects of the reaction pose problems of both O_2 access after the active site is blocked by substrate and cleavage specificity, since the entire aromatic ring system is presumably electron-rich following ionization of the phenolate groups. Our structures suggest that these problems are solved in 3,4-PCD by coupling the substrate binding/activation process to the creation of a sequestered O_2 binding site immediately adjacent to the bonds in PCA where cleavage will occur (Figures 5 and 6c). Access to this site may occur through a path along the α-subunit−β-subunit interface which leads directly into the cavity and undergoes structural perturbations upon formation of the enzyme·PCA complex as indicated in Figures 1a and 2. The binding of O_2 in this cavity is supported by the observation that CN^- binds in this site in the ternary complexes (Figure 7e). However, it should be pointed out that the coordination of CN^- to the Fe^{3+} is fundamentally different than our proposal for O_2 binding in the cavity prior to reaction with PCA. Interestingly, CN^- binds in an unexpected nonlinear conformation due to steric constraints within the binding pocket. Similar considerations of bond linearity are not relevant in the case of O_2 because it will not coordinate to the iron as long as it remains Fe^{3+}. However, following O_2 attack on the PCA^{C4}, the oxygen will take on peroxide character and would readily coordinate to the iron in the open binding site (Figure 7f). This Fe−O−O−PCA intermediate would necessarily have a nonlinear Fe−O−O bond angle and is consistent with the shape of the cavity. Triplet O_2 has a 1.21 Å O−O bond distance that increases to 1.48 Å in H_2O_2 with a H−O−O bond angle of approximately 100° (Cotton & Wilkinson, 1988). These parameters are remarkably consistent with the dimensions of the putative O_2 cavity and the energy-minimized peroxy intermediate model shown in Figure 7f. The *R* configuration at PCA^{C4} for the proposed tridentate peroxy intermediate has a structural precedence in the noncatalytic Ir^{3+}·catecholate·O_2 model complexes (Barbaro et al., 1991, 1992).

We propose in the mechanistic cycle of Figure 8 that the asymmetry and chirality of the active site and peroxy intermediate are responsible for concomitant O−O bond cleavage and insertion into the PCA C3−C4 bond. The active site cavity guides PCA into iron coordination sites with PCA^{O3} and PCA^{O4} groups opposite $Tyr408^{O\eta}$ and $His462^{N\epsilon2}$, respectively. A *trans* influence reduces the PCA^{O4}−Fe^{3+} bond distance by accepting electron density into His462 and increases the PCA^{O3}−Fe^{3+} bond distance as Tyr408 donates electron density to the iron. These *trans* influences are observed in the Fe^{3+}·PCA and Fe^{3+}·INO bond distances illustrated in panels d and e of Figure 7, respectively. When O_2 binds, these distortions, as well as the hydrogen bond between $Arg457^{N\eta1}$ and PCA^{O3}, enhance both the tendency of PCA^{O3} to ketonize and the carbanion character at PCA^{C4}. This reduces the double bond character of the scissile C3−C4 bond in PCA and leads to electrophilic attack of O_2 on the *si* face at PCA^{C4}. Subsequently, the distal end of the peroxy intermediate coordinates to the iron opposite $His460^{N\epsilon2}$ (Figure 7f) where another *trans* influence

may induce O−O bond cleavage. We propose that together these concerted *trans* influences facilitate O_2 bond cleavage and insertion into the PCA C3−C4 bond to yield the proposed anhydride intermediate.

Transient kinetic studies suggest rapid hydrolysis of the anhydride intermediate to yield a product complexed with the Fe^{3+} (Fujisawa et al., 1971, 1972; Bull et al., 1981). The reaction stoichiometry requires that this process involves the second oxygen atom from O_2 which is proposed to be retained in the O_2 cavity by coordination to the iron. Although our structures suggest that the O_2 cavity is sequestered from bulk solvent, the 3,4-PCD·INO/NNO·CN complexes each contain a solvent molecule (Wat606) at the bottom of the cavity in addition to CN^- (Figure 6c). Hydrolysis of the anhydride by the Fe^{3+}−oxide/hydroxide species is proposed to be faster than exchange with Wat606 for most substrates because several hydrogen bonds hold Wat606 in place. However, when 3,4-PCD or 1,2-CTD turns over pyrogallol, solvent exchange is occasionally observed (Saeki et al., 1980; Mayer & Que, 1984) since the turnover is at least 400 times slower than that for the natural substrates.

The rate-limiting process in turnover for 3,4-PCD is product release ($\sim$36 s^{-1}, turnover number $\approx$ 40 s^{-1}) (Fujisawa et al., 1971, 1972; Bull et al., 1981). The tridentate product complex illustrated in Figure 8 is geometrically reasonable, although charge repulsion of the product carboxylate groups will make this an unstable structure. This is supported by the observation that free product has a very low affinity for the enzyme. We are currently analyzing several crystal structures of dicarboxylate-containing product analogs of 3,4-PCD which show direct coordination to the iron but no release of Tyr447. Therefore, it seems reasonable to presume that, as β-carboxy-*cis,cis*-muconate dissociates from the iron, it facilitates the deprotonation of Tyr447 and perhaps a solvent molecule. The tyrosinate and hydroxide would then coordinate the iron to regenerate the resting state of enzyme.

What Is the Nature of the "Activated" PCA Species? Ketonization of PCA has been considered to be an important aspect of the mechanism of 3,4-PCD since the first mechanistic proposals based on an active site Fe^{3+} were advanced (Que et al., 1976; Whittaker & Lipscomb, 1984b). Ketonization must occur for a mechanism in which O_2 attacks the activated substrate, but it is unclear whether ketonization is a necessary aspect of the activation or whether it results from attack of O_2 on one of the ring carbons. We have argued here that endogenous *trans* ligand influences in the iron coordination sphere will promote inequivalent Fe^{3+}·-catecholate bonds in PCA, which will consequently favor ketonization in the enzyme·substrate complex. INO and NNO are known from spectroscopic studies to bind to the enzyme in the ketonized tautomer (Whittaker & Lipscomb, 1984b). However, PCA binds with very similar Fe^{3+}−ligand bond distances to these inhibitors so that the differences only become apparent after averaging the six active site metal centers. On the other hand, the spectroscopic properties of the *N*-oxide inhibitor complexes with 3,4-PCD are markedly different from those of the 3,4-PCD·PCA complex, suggesting that the electronic nature of the inhibitor complexes is quite different than that of the PCA complex. The structures reported here show that the *N*-oxide inhibitor complexes have a solvent in the sixth coordination site, whereas this site is apparently unoccupied in the PCA complex. Together, these observations suggest that PCA binds in a favorable position to eventually ketonize, but is not fully ketonized in the anaerobic enzyme·substrate complex. The dianionic nature of the chelated PCA·Fe^{3+} complex would, nevertheless, still effectively promote electrophilic attack by O_2. The spectral properties of the INO and NNO complexes faithfully reproduce those of the intermediate that forms immediately after O_2 is introduced to the 3,4-PCD·PCA complex. In the mechanism illustrated in Figure 8, the 3,4-PCD·PCA·peroxy intermediate species involves a ketonized PCA·Fe^{3+} complex in which the distal oxygen of the peroxy molecule coordinates to the iron as illustrated in Figure 7f. The similarity between this intermediate structure and that of the binary *N*-oxide inhibitor complexes would likely produce very similar electronic environments for the iron and consequently yield equivalent spectroscopic properties. This also suggests that the bound solvent molecule in the structures of the *N*-oxide complexes is hydroxide rather than a neutral water ligand in order for maintaining the overall charge neutrality of the metal center.

All spectroscopic results indicate that the iron of 3,4-PCD remains ferric throughout the reaction cycle, but studies of some inorganic model complexes that catalyze intradiol ring cleavage of catecholic substrates indicate that a Fe^{2+}·-semiquinone complex is also a reasonable description of the activated substrate species (Cox & Que, 1988; Jang et al., 1991). Such a species might allow O_2 to bind directly to the iron as in the Fe^{2+} dioxygenases, or it might facilitate the direct one-step attack of triplet oxygen by giving the substrate radical character. However, structural comparisons of the enzyme and the $[Fe(TPA)DBC]^+$ model complex suggest several significant differences. The TPA tripodal ligand yields essentially planar chelated catecholates bound to the octahedrally coordinated iron. The approximately symmetric Fe^{3+}−catecholate bonds are only about 0.1 Å different in length. Our enzyme structures, in contrast, suggest more asymmetric ($\Delta r \sim 0.2-0.4$ Å) chelated Fe^{3+}·-catecholate complexes that result in part from the nature of the endogenous *trans* ligands discussed above. The Fe^{3+} is also significantly ($\sim$0.8−1.2 Å) out of the substrate plane (Table 4) in the enzyme active site. The enzyme reserves an iron coordination site adjacent to PCA that can potentially participate in the chemical reaction, whereas the model complexes have all ligand sites filled. The nitrogen-rich ligands in the most active model complexes serve to increase the Lewis acidity of the iron, and consequently, the model complexes are more likely to yield the Fe^{2+}·semiquinone species. By comparison, the ligand set of the 3,4-PCD·-PCA complex revealed here will produce a much less Lewis acidic iron which will be difficult to reduce by the relatively high potential catecholate substrate ligands. Considered together, the structural data support the spectroscopic observations that the iron does not become reduced during the catalytic cycle.

Structurally Based Sequence Alignment of Intradiol-Cleaving Catecholic Dioxygenases. The three-dimensional structures of the *P. putida* 3,4-PCD as isolated (Ohlendorf et al., 1994) and the numerous ligand complexes in this and the preceding paper (Orville et al., 1997) are ideal reference points for examining amino acid sequence alignments for the family of intradiol-cleaving catecholic dioxygenases as summarized in Figure 9. Recently, Gerischer and Ornston (1995) reported a genetic selection strategy that utilizes

	source[a] enzyme	active site perimeter										mid-site α			mid-site β			near Fe^{3+}				Fe^{3+} ligands			
1	*A.c.* 1,2-CTD	Y_{83}	L_{84}	D_{85}	D_{232}	G_{233}	P_{169}	T_{170}	P_{203}			I_{105}	E_{106}	G_{107}	C_{201}	Y_{255}		P_{108}	L_{109}	W_{156}	R_{221}	Q_{240}	Y_{164}	Y_{200}	H_{224}	H_{226}
2	*P.sp.* 1,2-CTD	Y_{83}	M_{84}	D_{85}	P_{229}	G_{230}	K_{169}	S_{170}	P_{200}			I_{105}	E_{106}	G_{107}	V_{199}	F_{252}		P_{108}	L_{109}	W_{156}	R_{218}	Q_{237}	Y_{164}	Y_{197}	H_{221}	H_{223}
3	*P.p.* 1,2-CTD	F_{82}	L_{83}	D_{84}	P_{228}	G_{229}	S_{167}	T_{168}	D_{199}			I_{104}	E_{105}	G_{106}	C_{198}	Y_{251}		P_{107}	L_{108}	W_{154}	R_{217}	Q_{236}	Y_{162}	Y_{196}	H_{220}	H_{222}
4	*P.a.* 1,2-CTD β	F_{82}	L_{83}	D_{84}	P_{228}	G_{229}	S_{167}	T_{168}	D_{199}			I_{104}	E_{105}	G_{106}	C_{198}	Y_{251}		P_{107}	L_{108}	W_{154}	R_{217}	Q_{236}	Y_{162}	Y_{196}	H_{220}	H_{222}
5	*A.sp.* 1,2-CTD	W_{83}	V_{84}	E_{85}	P_{228}	G_{229}	P_{168}	G_{169}	P_{199}			I_{104}	E_{105}	G_{106}	I_{198}	S_{251}		P_{107}	Y_{108}	W_{155}	R_{217}	Q_{236}	Y_{163}	Y_{196}	H_{220}	H_{222}
6	*P.sp.* 1,2-CTD	F_{53}	F_{54}	N_{55}	D_{196}	G_{197}	D_{135}	Q_{136}	P_{167}			M_{73}	Q_{74}	G_{75}	I_{166}	K_{249}		P_{76}	Y_{77}	W_{122}	R_{184}	Q_{234}	Y_{130}	Y_{194}	H_{188}	H_{190}
7	*P.sp.* Cl-CTD	F_{53}	L_{54}	N_{55}	D_{196}	G_{197}	D_{135}	N_{136}	P_{167}			I_{73}	Q_{74}	G_{75}	I_{166}	H_{219}		P_{76}	Y_{77}	W_{122}	R_{184}	Q_{204}	Y_{130}	Y_{194}	H_{188}	H_{190}
8	*A.e.* Cl-CTD	F_{53}	F_{54}	N_{55}	P_{196}	G_{197}	D_{135}	D_{136}	P_{167}			I_{73}	E_{74}	G_{75}	I_{166}	N_{219}		P_{76}	Y_{77}	W_{122}	R_{184}	Q_{204}	Y_{130}	Y_{194}	H_{188}	H_{190}
9	*P.c.* 3,4-PCD β	**Y_{23}**	**R_{24}**	**S_{25}**	D_{167}	Y_{168}	**D_{112}**	**Q_{113}**	**G_{149}**			Q_{45}	Y_{46}	A_{47}	**W_{148}**	**I_{190}**		P_{48}	V_{49}	**W_{99}**	**R_{156}**	**Q_{176}**	**Y_{107}**	**Y_{146}**	**H_{159}**	**H_{161}**
10	*A.c.* 3,4-PCD β	**Y_{25}**	**K_{26}**	**T_{27}**	D_{169}	G_{170}	**D_{114}**	**Q_{115}**	**R_{151}**			V_{47}	T_{48}	A_{49}	**W_{150}**	**I_{192}**		P_{50}	H_{51}	**W_{101}**	**R_{158}**	**Q_{178}**	**Y_{109}**	**Y_{148}**	**H_{161}**	**H_{163}**
11	***P.p.* 3,4-PCD β**	**Y_{24}**	**K_{25}**	**T_{26}**	P_{167}	S_{168}	**D_{113}**	**R_{114}**	**R_{150}**			T_{46}	T_{47}	G_{48}	W_{149}	I_{191}		P_{49}	N_{50}	W_{100}	R_{157}	Q_{177}	**Y_{108}**	**Y_{147}**	**H_{160}**	**H_{162}**
12	***P.p.* 3,4-PCD α**	-	-	-	**R_{133}**	**G_{134}**	D_{81}	-	A_{117}			**T_{12}**	**A_{13}**	**G_{14}**	N_{116}	V_{157}		**P_{15}**	**Y_{16}**	W_{71}	M_{122}	R_{142}	Y_{79}	V_{114}	H_{125}	N_{127}
13	*A.c.* 3,4-PCD α	-	-	-	**R_{142}**	**G_{143}**	D_{88}	T_{89}	R_{126}			**T_{16}**	**G_{17}**	**G_{18}**	G_{125}	V_{166}		**P_{19}**	**Y_{20}**	W_{75}	Q_{131}	R_{151}	Y_{83}	V_{123}	H_{134}	S_{136}
14	*P.c.* 3,4-PCD α	-	-	-	**R_{130}**	**G_{131}**	D_{82}	D_{83}	-			**T_{11}**	**V_{12}**	**G_{13}**	-	V_{154}		**P_{14}**	**Y_{15}**	T_{69}	E_{119}	R_{139}	F_{77}	I_{115}	H_{122}	N_{124}
	proposed function	aromatic substrate specificity																catalysis and F^{3+} stabilization								

FIGURE 9: Alignment of active site residues in Fe^{3+} catecholic dioxygenases based on the structure of the *P. putida* 3,4-PCD·PCA complex. The shaded residues are within approximately 8 Å of PCA. The primary sequences were aligned and adjusted slightly to reinforce the three-dimensional structural homology between the α- and β-subunits of *P. putida* 3,4-PCD. The enzymes are from the following references: (1) *catA, Acinetobacter calcoaceticus* (Neidle et al., 1988); (2) *pheB, Pseudomonas* sp. (Kivisaar et al., 1991); (3) *catA, P. putida* (mt-2) (Nakai et al., 1995); (4) *catA, Pseudomonas arvilla* (c-1), β-chain (Nakai et al., 1995); (5) *catA, Arthrobacter sp.* (Eck & Belter, 1993); (6) *tcbC, Pseudomonas* sp. (van der Meer et al., 1991); (7) *clcA, Pseudomonas sp.* (Frantz & Chakrabarty, 1987); (8) *tfdC, Alcaligenes eutrophus* (Perkins et al., 1990); (9) *pcaA, Pseudomonas cepacia,* β-chain (Zylstra et al., 1989); (10) *pcaH, A. calcoaceticus,* β-chain (Hartnett et al., 1990); (11) *pcaH, P. putida,* β-chain (Frazee et al., 1993); (12) *pcaG, P. putida,* α-chain (Frazee et al., 1993); (13) *pcaG, A. calcoaceticus,* α-chain (Hartnett et al., 1990); and (14) *pcaA, P. cepacia,* α-chain (Zylstra et al., 1989).

spontaneous mutations to the 3,4-PCD structural genes from *A. calcoaceticus* to select for strains with abolished or greatly reduced 3,4-PCD activity. It is interesting to note that several of the mutants from this study include single-amino acid substitution at important positions in our sequence alignment.

The sequence alignment suggests that substrate specificity within the family is governed by several residues around the active site periphery. For example, $Tyr324^{OH}$ (Y24β) in 3,4-PCD forms a strong hydrogen bond with the carboxylate group of PCA. In three out of five 1,2-CTDs and both known Cl-CTDs, Tyr324 is replaced by either Phe or Trp. The positively charged residues in 3,4-PCD, Arg133 (R133α), Lys325 (K25β), and Arg450 (R150β), are replaced by either hydrophobic or negatively charged residues in the 1,2-CTD and Cl-CTD sequences. Finally, Ala13 (A13α) and Thr326 (T26β) in 3,4-PCD are replaced by acidic residues in most of the 1,2-CTDs. Together, these residues in 1,2-CTD and Cl-CTD are expected to favor an increased affinity for more hydrophobic substrates and concomitantly reduce the electrostatic attraction of negatively charged substrates such as PCA to the active site.

The sequence alignment also suggests that Cys198 or Cys201 in 1,2-CTD isolated from either *A. calcoaceticus*, *P. putida* (mt-2), or *P. arvilla* (C-1) is in a location analogous to Trp449 (W149β) in 3,4-PCD. This residue forms one side of the active site in 3,4-PCD and influences the PCA binding orientation. Accordingly, the *P. arvilla* (C-1) 1,2-CTD catalytic activity is eliminated by treatment with *p*-chloromercuribenzoate (pCMB) (Nagami, 1972), while 3,4-PCD from *P. putida* remains active (Fujisawa & Hayaishi, 1968).

The mechanism presented here emphasizes the important roles played by the iron ligands in activating the substrate and promoting the insertion chemistry. All the endogenous Fe^{3+} ligands appear to be conserved in every member of the Fe^{3+} dioxygenase family. Frazee (1994) showed that site-directed mutants at Tyr447 (Y147β) all have greatly reduced or abolished catalytic activity. Moreover the detailed transient kinetic and crystallographic analysis of the Tyr447 → His mutant 3,4-PCD[6] corroborates the importance of Tyr447 in the reaction mechanism and rationalizes its absolute conservation in other members of the family. Several other potentially important residues have also been identified in the current study and are found to be conserved in the other Fe^{3+} dioxygenases as well. The absolutely conserved Arg457 (R157β) is ideally positioned to align substrate and stabilize a developing negative charge at the PCA C4−C3 bond. The position of Arg457 is held in this critical orientation by hydrogen bonding to Gln477 (Q177β), which is also strictly conserved.

Since formation of a ternary enzyme·substrate·O_2 complex is critical for catalysis, the residues around the putative O_2 binding cavity should be very highly conserved in all the enzymes in the family. The sequence alignments suggest that these residues, including Gly14 (G14α), Pro15 (P15α),

[6] R. W. Frazee, A. M. Orville, K. B. Dolbeare, Y. Hong, D. H. Ohlendorf, and J. D. Lipscomb, in preparation.

Tyr16 (Y16α), Trp400 (W10β), and Tyr447 (Y147β), are indeed completely conserved with the exception of Tyr16 which is conserved in all 3,4-PCDs and most of the other related enzymes. In some 1,2-CTDs, Leu is substituted in this position. However, the main chain and side chain atoms of Leu could serve an analogous structural role as Tyr16 in providing part of the equatorial wall of the O_2 binding cavity.

Relevance to Other Metalloenzymes. We have shown here that endogenous iron ligand displacement is caused by substrate binding to the iron in 3,4-PCD. It is likely that both this process and the ability of the iron coordination number to change dynamically during turnover are critical for the function of this and other members in the family of intradiol-cleaving catecholic dioxygenases. Recently, crystal structures and mechanistic studies of several other mononuclear iron-containing enzymes, including iron superoxide dismutase (Lah et al., 1995; Tierney et al., 1995), 2,3-dihydroxybiphenyl 1,2-dioxygenase (Sugiyama et al., 1995; Han et al., 1995; Senda et al., 1996), isopenicillin *N*-synthase (Roach et al., 1995; Orville et al., 1992; Randall et al., 1993), and soybean lipoxygenase (Boyington et al., 1993; Minor et al., 1993, 1996; Pavlosky et al., 1995; Nelson et al., 1995), have been reported. Although the structures of these other enzymes complexed with a variety of exogenous ligands have not been examined in the detail we report here for 3,4-PCD, many common mechanistic themes are emerging [for recent reviews, see Holm et al. (1996) and Que and Ho (1996)]. For one or more of the cited examples, these include (i) direct coordination of substrates to the iron as an important part of the chemical mechanism, (ii) dissociation of endogenous ligands in response to exogenous ligand binding, (iii) expansion of the coordination sphere during catalysis, and (iv) creation of binding sites for small molecules either on the metal or nearby in response to substrate binding. 3,4-PCD provides the best example currently available of the coordinated application of all these aspects of metalloprotein catalysis.

ACKNOWLEDGMENT

We thank Dr. L. Que, Jr., and M. Vetting for many insightful discussions. We also thank the Minnesota Supercomputer Institute for providing computational resources and E. Hoeffner for maintenance of the facilities in the Kahlert Structural Biology Laboratory at the University of Minnesota.

REFERENCES

Arciero, D. M., & Lipscomb, J. D. (1986) *J. Biol. Chem. 261*, 2170−2178.

Arnez, J. G. (1994) *J. Appl. Crystallogr. 27*, 649−653.

Barbaro, P., Bianchini, C., Mealli, C., & Meli, A. (1991) *J. Am. Chem. Soc. 113*, 3181−3183.

Barbaro, P., Bianchini, C., Frediani, P., Meli, A., & Vizza, F. (1992) *Inorg. Chem. 31*, 1523−1529.

Bernstein, F. C., Koetzle, T. F., Williams, G. J. B., Meyer, E. F., Jr., Brice, M. D., Rodgers, J. R., Kennard, O., Shimanouchi, T., & Tasumi, M. (1977) *J. Mol. Biol. 112*, 535−542.

Boyington, J. C., Gaffney, B. J., & Amzel, L. M. (1993) *Science 260*, 1482−1486.

Broderick, J. B., & O'Halloran, T. V. (1991) *Biochemistry 30*, 7349−7358.

Bull, C., Ballou, D. P., & Otsuka, S. (1981) *J. Biol. Chem. 256*, 12681−12686.

Cotton, F. A., & Wilkinson, G. (1988) in *Advanced Inorganic Chemistry*, 5th ed., pp 449−460, John Wiley & Sons, Inc., New York.

Cox, D. D., & Que, L., Jr. (1988) *J. Am. Chem. Soc. 110*, 8085−8092.

Dagley, S. (1977) *Surv. Prog. Chem. 8*, 121−170.

Dagley, S. (1978) in *The Bacteria* (Ornston, L. N., & Sokatch, J. R., Eds.) Vol. 6, pp 305−388, Academic Press, New York.

Felton, R. H., Gordon, S. L., Sowell, A. L., & May, S. W. (1984) *Biochemistry 23*, 3955−3959.

Ferrin, T. E., Huang, C. C., Jarvis, L. E., & Langridge, R. (1988) *J. Mol. Graphics 6*, 13−27.

Frazee, R. W. (1994) Doctoral Dissertation, University of Minnesota, Minneapolis, MN.

Frazee, R. W., Livingston, D. M., LaPorte, D. C., & Lipscomb, J. D. (1993) *J. Bacteriol. 175*, 6194−6202.

Fujisawa, H., & Hayaishi, O. (1968) *J. Biol. Chem. 243*, 2673−2681.

Fujisawa, H., Hiromi, K., Uyeda, M., Nozaki, M., & Hayaishi, O. (1971) *J. Biol. Chem. 246*, 2320−2321.

Fujisawa, H., Hiromi, K., Uyeda, M., Okuno, S., Nozaki, M., & Hayaishi, O. (1972) *J. Biol. Chem. 247*, 4422−4428.

Gerischer, U., & Ornston, L. N. (1995) *J. Bacteriol. 177*, 1336−1347.

Glusker, J. P. (1991) *Adv. Protein Chem. 42*, 1−76.

Han, S., Eltis, L. D., Timmis, K. N., Muchmore, S. W., & Bolin, J. T. (1995) *Science 270*, 976−980.

Harayama, S., Kok, M., & Neidle, E. L. (1992) *Annu. Rev. Microbiol. 46*, 565−601.

Hartnett, C., Neidle, E. L., Ngai, K.-L., & Ornston, N. L. (1990) *J. Bacteriol. 172*, 956−966.

Hendrickson, W. A. (1985) *Methods Enzymol. 115*, 252−270.

Hendrickson, W. A., & Konnert, J. H. (1980) in *Biomolecular Structure, Function, Conformation and Evolution* (Srinvasan, R., Ed.) Vol. 1, pp 43−47, Pergamon, Oxford.

Holm, R. H., Kennepohl, P., & Solomon, E. I. (1996) *Chem. Rev. 96*, 2239−2314.

Hooft, R. W. W., Vriend, G., Sander, C., & Abola, E. E. (1996) *Nature 381*, 272.

Hou, C.-T. (1975) *Biochemistry 14*, 3899−3902.

Jang, H. G., Cox, D. D., & Que, L., Jr. (1991) *J. Am. Chem. Soc. 113*, 9200−9204.

Jones, T. A. (1978) *J. Appl. Crystallogr. 11*, 268−272.

Kraulis, P. J. (1991) *J. Appl. Crystallogr. 24*, 946−950.

Lah, M. S., Dixon, M. M., Pattridge, K. A., Stallings, W. C., Fee, J. A., & Ludwig, M. L. (1995) *Biochemistry 34*, 1646−1660.

Laskowski, R. A., MacArthur, M. W., Moss, S. D., & Thornton, J. M. (1993) *J. Appl. Crystallogr. 26*, 283−291.

Lauffer, R. B., & Que, L., Jr. (1982) *J. Am. Chem. Soc. 104*, 7324−7325.

Lipscomb, J. D., & Orville, A. M. (1992) in *Metal Ions in Biological Systems* (Sigel, H., & Sigel, A., Eds.) Vol. 28, pp 243−298, Marcel Dekker, Inc., New York.

Lipscomb, J. D., Whittaker, J. W., & Arciero, D. M. (1982) in *Oxygenases and Oxygen Metabolism* (Nozaki, M., Yamamoto, S., Ishimura, Y., Coon, M. J., Ernster, L., & Estabrook, R. W., Eds.) pp 27−38, Academic Press, Inc., New York.

Luzzati, V. (1952) *Acta Crystallogr. 5*, 802−810.

Mabrouk, P. M., Orville, A. M., Lipscomb, J. D., & Solomon, E. I. (1991) *J. Am. Chem. Soc. 113*, 4053−4061.

May, S. W., & Phillips, R. S. (1979) *Biochemistry 18*, 5933−5939.

May, S. W., Phillips, R. S., & Oldham, C. D. (1978) *Biochemistry 17*, 1853−1860.

May, S. W., Oldham, C. D., Mueller, P. W., Padgette, S. R., & Sowell, A. L. (1982) *J. Biol. Chem. 257*, 12746−12751.

Mayer, R. J., & Que, L., Jr. (1984) *J. Biol. Chem. 259*, 13056−13060.

Minor, W., Steczko, J., Bolin, J. T., Otwinowski, Z., & Axelrod, B. (1993) *Biochemistry 32*, 6320−6323.

Minor, W., Steczko, J., Stec, B., Otwinowski, Z., Bolin, J. T., Walter, R., & Axelrod, B. (1996) *Biochemistry 35*, 10687−10701.

Nagami, K. (1972) *Biochem. Biophys. Res. Commun. 47*, 803−807.

Nakai, C., Uyeyama, H., Kagamiyama, H., Nakazawa, T., Inouye, S., Kishi, F., Nakazawa, A., & Nozaki, M. (1995) *Arch. Biochem. Biophys. 321*, 353−362.

Nelson, M. J., Brennan, B. A., Chase, D. B., Cowling, R. A., Groove, G. N., & Scarrow, R. C. (1995) *Biochemistry 34*, 15219−15229.
Ohlendorf, D. H., Weber, P. C., & Lipscomb, J. D. (1987) *J. Mol. Biol. 195*, 225−227.
Ohlendorf, D. H., Lipscomb, J. D., & Weber, P. C. (1988) *Nature 336*, 403−405.
Ohlendorf, D. H., Orville, A. M., & Lipscomb, J. D. (1994) *J. Mol. Biol. 244*, 586−608.
Orville, A. M., & Lipscomb, J. D. (1989) *J. Biol. Chem. 264*, 8791−8801.
Orville, A. M., & Lipscomb, J. D. (1993) *J. Biol. Chem. 268*, 8596−8607.
Orville, A. M., Chen, V. C., Kriauciunas, A., Harpel, M. R., Fox, B. G., Münck, E., & Lipscomb, J. D. (1992) *Biochemistry 31*, 4602−4612.
Orville, A. M., Elango, N., Lipscomb, J. D., & Ohlendorf, D. H. (1997) *Biochemistry 36*, 10039−10051.
Pavlosky, M. A., Zhang, Y., Westre, T. E., Gan, Q.-F., Pavel, E. G., Campochiaro, C., Hedman, B., Hodgson, K. O., & Solomon, E. I. (1995) *J. Am. Chem. Soc. 117*, 4316−4327.
Que, L., Jr. (1989) in *Iron Carriers and Iron Proteins* (Loehr, T. M., Ed.) pp 467−524, VCH, New York.
Que, L., Jr., & Ho, R. Y. N. (1996) *Chem. Rev. 96*, 2607−2624.
Que, L., Jr., Lipscomb, J. D., Zimmermann, R., Münck, E., Orme-Johnson, N. R., & Orme-Johnson, W. H. (1976) *Biochim. Biophys. Acta 452*, 320−334.
Randall, C. R., Zang, Y., True, A. E., Que, L., Jr., Charnock, J. M., Garner, C. D., Fujishina, Y., Schofield, C. J., & Baldwin, J. E. (1993) *Biochemistry 32*, 6644−6673.
Roach, P. L., Clifton, I. J., Fülöp, V., Harlos, K., Barton, G. J., Hajdu, J., Andersson, I., Schofield, C. J., & Baldwin, J. E. (1995) *Nature 375*, 700−704.
Saeki, Y., Nozaki, M., & Senoh, S. (1980) *J. Biol. Chem. 255*, 8465−8471.
Senda, T., Sugiyama, K., Narita, H., Yamamoto, T., Kimbara, K., Fukuda, M., Sato, M., Yano, K., & Mitsui, Y. (1996) *J. Mol. Biol. 255*, 735−752.
Shu, L., Chiou, Y.-M., Orville, A. M., Miller, M. A., Lipscomb, J. D., & Que, L. Jr. (1995) *Biochemistry 34*, 6649−6659.
Siu, D. C.-T., Orville, A. M., Lipscomb, J. D., Ohlendorf, D. H., & Que, L., Jr. (1992) *Biochemistry 31*, 10443−10448.
Smith, R. H., & Martell, A. E. (1989) in *Critical Stability Constants*, Vol. 6, Plenum Press, New York (supplemental no. 2 and earlier volumes).
Sugiyama, K., Senda, T., Narita, H., Yamamoto, T., Kimbara, K., Fukuda, M., Yano, K., & Mitsui, Y. (1995) *Proc. Jpn. Acad., Ser. B 71*, 32−35.
Tierney, D. L., Fee, J. A., Ludwig, M. L., & Penner-Hahn, J. E. (1995) *Biochemistry 34*, 1661−1668.
True, A. E., Orville, A. M., Pearce, L. L., Lipscomb, J. D., & Que, L., Jr. (1990) *Biochemistry 29*, 10847−10854.
Tyson, C. A. (1975) *J. Biol. Chem. 250*, 1765−1770.
Vetting, M. W., Earhart, C. A., & Ohlendorf, D. H. (1994) *J. Mol. Biol. 236*, 372−373.
Whittaker, J. W., & Lipscomb, J. D. (1984a) *J. Biol. Chem. 259*, 4487−4495.
Whittaker, J. W., & Lipscomb, J. D. (1984b) *J. Biol. Chem. 259*, 4476−4486.
Whittaker, J. W., Lipscomb, J. D., Kent, T. A., & Münck, E. (1984) *J. Biol. Chem. 259*, 4466−4475.
Zylstra, G. J., Olsen, R. H., & Ballou, D. P. (1989) *J. Bacteriol. 171*, 5915−5921.

BI970469F